REPORT DOCUMENTATION PAGE

Form Approved
OMB No. 0704-0188

1. REPORT DATE *(DD-MM-YYYY)*	**2. REPORT TYPE**	**3. DATES COVERED** *(From - To)*
15-4-08	Final Report	5/1/05-10/31/07

4. TITLE AND SUBTITLE
Novel Wavelength Standards in the Near Infrared

5a. CONTRACT NUMBER
FA9550-05-1-0304

5b. GRANT NUMBER
BG0764

5c. PROGRAM ELEMENT NUMBER

6. AUTHOR(S)
Corwin, Kristan L.

5d. PROJECT NUMBER
GOPY530764

5e. TASK NUMBER

5f. WORK UNIT NUMBER

7. PERFORMING ORGANIZATION NAME(S) AND ADDRESS(ES) AND ADDRESS(ES)
Kansas State University
Department of Physics
116 Cardwell Hall
Manhattan, KS 66506

8. PERFORMING ORGANIZATION REPORT NUMBER

9. SPONSORING / MONITORING AGENCY NAME(S) AND ADDRESS(ES)
Air Force Office of Scientific Research
875 North Randolph St.
Ste 325 Rm 3112
Arlington, VA 22203

10. SPONSOR/MONITOR'S ACRONYM(S)
AFOSR

11. SPONSOR/MONITOR'S REPORT NUMBER(S)

12. DISTRIBUTION / AVAILABILITY STATEMENT
UNLIMITED

13. SUPPLEMENTARY NOTES

14. ABSTRACT

The goal of this work is to develop a new class of portable optical frequency references based on sub-Doppler spectroscopy inside gas-filled hollow-core photonic bandgap optical fiber. This research has three major components, consisting of spectroscopy in hollow fiber, the development of a near-IR optical frequency comb with which to characterize the transitions inside the fiber, and efforts to seal these fibers filled with molecular gases to create portable frequency references. Sub-Doppler spectra were observed for the first time in such fibers, and the dependence of the feature width on fiber core diameter was established. A mode-locked chromium-doped forsterite laser based on prism pair dispersion compensation was stabilized as an optical frequency comb for the first time, and unique noise properties were identified. Dramatic narrowing of the carrier-envelope offset frequency (f_0) was observed when a knife-edge was inserted in the optical cavity. Finally, new fusion splicing techniques for hollow-core photonic bandgap optical fiber were developed.

15. SUBJECT TERMS
Optical frequency combs, hollow photonic bandgap fiber, microstructured or photonic crystal fiber, saturated absorption spectroscopy, portable wavelength standards or references

16. SECURITY CLASSIFICATION OF:			**17. LIMITATION OF ABSTRACT**	**18. NUMBER OF PAGES**	**19a. NAME OF RESPONSIBLE PERSON**
					Kristan Corwin
a. REPORT	**b. ABSTRACT**	**c. THIS PAGE**	UU	54	**19b. TELEPHONE NUMBER** *(include area code)*
U	U	U			785-532-1663

Final Report

"Novel Wavelength Standards in the Near IR"

Award Number: **FA9550-05-1-0304**

Time period: **May 1, 2005 – October 31, 2007**

PI: **Dr. Kristan L. Corwin**

Institution: **Kansas State University**

Address: **Department of Physics**
116 Cardwell Hall
Manhattan, KS 66506

Phone: **(785) 532-1663**

Abstract: (200 word maximum)

The goal of this work is to develop a new class of portable optical frequency references based on sub-Doppler spectroscopy inside gas-filled hollow-core photonic bandgap optical fiber. This research has three major components, consisting of spectroscopy in hollow fiber, the development of a near-IR optical frequency comb with which to characterize the transitions inside the fiber, and efforts to seal these fibers filled with molecular gases to create portable frequency references. Sub-Doppler spectra were observed for the first time in such fibers, and the dependence of the feature width on fiber core diameter was established. A mode-locked chromium-doped forsterite laser based on prism pair dispersion compensation was stabilized as an optical frequency comb for the first time, and unique noise properties were identified. Dramatic narrowing of the carrier-envelope offset frequency (f_0) was observed when a knife-edge was inserted in the optical cavity. Finally, new fusion splicing techniques for hollow-core photonic bandgap optical fiber were developed.

Objectives:

- To improve portable optical frequency references in the near infrared spectral region.
- To develop novel frequency references based on photonic band gap (PBG) fiber.
- To demonstrate and fully characterize saturation spectroscopy features inside PBG fiber.
- To minimize the linewidth while maximizing the signal strength inside these PBG fibers.
- To seal acetylene inside PBG fiber cells without introducing any impurities, by improving fusion splicing techniques for PBG fibers.
- To characterize the short-term stability and long-term accuracy of a cw laser locked to a saturated absorption feature in PBG fiber cell.
- To characterize a frequency comb that is locked to a PBG fiber cell.

Summary of major accomplishments:

The goal of this work is to develop a new class of portable optical frequency references based on sub-Doppler spectroscopy inside gas-filled hollow-core photonic bandgap optical fiber. This research has three major components, consisting of 1) spectroscopy in hollow fiber, 2) the development of a near-IR optical frequency comb with which to characterize the transitions inside the fiber, and 3) efforts to seal these fibers filled with molecular gases to create portable frequency references. We have made significant contributions in each of these areas.

Saturated Absorption: We were the first group to demonstrate sub-Doppler spectroscopy inside such a fiber [1]. Furthermore, we demonstrated the change in linewidth with core size [1-4], and have recently demonstrated narrower transitions inside a new "kagome" structured optical fiber which was provided to us through a collaboration with the University of Bath [5].

We have realized a simplified and more compact method for observing saturated absorption spectroscopy in half-sealed photonic bandgap fibers, [6, 7], called the "reflected pump technique," which was submitted as a provisional patent [8] but not as a full patent.

We have constructed two systems, each consisting of a narrow-line fiber laser locked to the P(13) transition in acetylene. By comparing those two systems, we will obtain stability data on the fiber-filled references.

Optical Frequency Comb: We have developed a mode-locked Cr:forsterite laser and stabilized it to a GPS-disciplined Rb clock with which to characterize the gas-filled hollow fiber optical frequency references [9]. We found that these lasers offer noisier "f_0" beats than Ti:sapphire lasers (just as a group at NIST had previously in chirped-mirror Cr:forsterite lasers), but also found a way to dramatically reduce that f_0 beat width [10, 11]. We have initiated a study into the source of the noise and the exact explanation for the narrowing. In the mean time, absolute frequency measurements of the fiber laser locked to the hollow fiber references are in progress.

Fiber Splicing: Together with Dr. Brian Washburn, we have developed a generally useful technique for splicing these photonic bandgap fibers to solid-core fibers using an arc fusion splicer, which makes PBG fibers easier to use in the laboratory [12, 13]. Toward making a completely sealed photonic bandgap fiber cell, we have also spliced PBG to solid-core fibers inside a vacuum system using a CO_2 laser. Unfortunately, efforts to reproduce this in an acetylene vapor have so far proved unsuccessful, most likely due to the thermal properties of acetylene. If this technique does not ultimately prove effective, we will use a He purge technique developed at the University of Bath to fabricate completely sealed fiber cells.

In summary, we have made important contributions to the development of portable optical frequency references based on acetylene-filled hollow optical fibers. Furthermore, we have observed interesting noise properties on a near-IR solid state laser that may have important consequences for better understanding of noise dynamics in optical frequency combs. All these developments may ultimately lead to improvements in portable optical frequency combs of moderate accuracy and stability locked to optical rather than microwave standards.

References

1. M. Faheem, R. Thapa, and K. L. Corwin, "Spectral Hole Burning of Acetylene Gas inside a Photonic Bandgap Optical Fiber," in *Conference on Lasers and Electro-optics*(Optical Society of America, Baltimore, MD, 2005).
2. R. Thapa, K. Knabe, M. Faheem, A. Naweed, O. L. Weaver, and K. L. Corwin, "Saturated absorption spectroscopy of acetylene gas inside large-core photonic bandgap fiber," Opt. Lett. **31**, 2489-2491 (2006).
3. R. Thapa, K. Knabe, A. Naweed, M. Faheem, O. L. Weaver, and K. L. Corwin, "Saturated Absorption Signals from Acetylene Gas Inside Photonic Bandgap Fiber," in *Conference on Lasers and Electro-Optics (CLEO)*(Long Beach, CA 2006).
4. K. Knabe, R. Thapa, O. L. Weaver, B. R. Washburn, and K. L. Corwin, "Comparison of Saturated Absorption Spectra of Acetylene Gas Inside Photonic Bandgap Fibers," in *Technical Digest: Symposium on Optical Fiber Measurement (SOFM)*(NIST, Boulder, CO, 2006).
5. K. Knabe, A. Jones, K. L. Corwin, F. Couny, P. S. Light, and F. Benabid, "Saturated Absorption Spectroscopy of C_2H_2 Inside a Hollow, Large-Core Kagome Photonic Crystal Fiber," in *Conference on Lasers and Electro-Optics (CLEO)*(OSA, San Jose, CA, 2008), p. JFA5.
6. K. Knabe, R. Thapa, B. R. Washburn, and K. L. Corwin, "Reflected Pump Technique for Fiber-based Saturated Absorption Spectroscopy," In preparation for Applied Optics (2008).
7. K. Knabe, R. Thapa, B. R. Washburn, and K. L. Corwin, "Reflected Pump Technique for Saturated Absorption Spectroscopy Inside Photonic Bandgap Fibers," in *Conference on Lasers and Electro-optics (CLEO)*(Optical Society of America, Baltimore, 2007).

8. K. Knabe, R. Thapa, B. R. Washburn, and K. L. Corwin, "Reflected Pump Technique for Saturated Absorption Spectroscopy inside Hollow Photonic Bandgap Fibers," *Provisional patent* (2006).
9. R. Thapa, K. A. Tillman, A. Naweed, A. Jones, B. R. Washburn, K. L. Corwin, J. W. Nicholson, and M. F. Yan, "Phase-stabilized Prism-based Cr:forsterite Laser Frequency Comb for Absolute Frequency Measurements," in *Conference on Lasers and Electro-Optics* (Optical Society of America, Baltimore, MD, 2007).
10. K. A. Tillman, R. Thapa, B. R. Washburn, and K. L. Corwin, "Carrier-envelope phase dynamics in a self-referenced prism-based chromium:forsterite frequency comb," in *Annual meeting of the Lasers for Electro-Optics Society (LEOS)*(Buena Vista, FL, 2007).
11. K. A. Tillman, R. Thapa, B. R. Washburn, and K. L. Corwin, "Significant Carrier Envelope Offset Frequency Linewidth Narrowing in a Prism-based Cr:forsterite Frequency Comb," in *Conference on Lasers and Electro-Optics (CLEO)*(Optical Society of America, San Jose, CA, 2008), p. CTuC5.
12. R. Thapa, K. L. Corwin, and B. R. Washburn, "Splicing Hollow-Core Photonic Bandgap Fiber to Step-Index Fibers Using an Arc Fusion Splicer," in *Conference on Lasers and Electro-Optics (CLEO)*(Optical Society of America, Long Beach, Calif., 2006).
13. R. Thapa, K. Knabe, K. L. Corwin, and B. R. Washburn, "Arc fusion splicing of hollow-core photonic bandgap fibers for gas-filled fiber cells " Opt. Express **14**, 9576-9583 (2006).

Personnel who worked on the project during the grant period: (those in bold are currently working on the project)

Faculty:	**Kristan L. Corwin (PI)**
Post-Docs:	Ahmer Naweed 1/05 – 5/06 (directly supported)
	Karl Tillman 9/06 - present (directly supported)
Graduate Students:	Mohammad Faheem (8/03 – 7/05), graduated with M.S.
	Andrew Jones (5/06 – present) (partial direct support)
	Rajesh Thapa (5/04 – Present) (partial direct support)
	Kevin Knabe (5/05– Present) (partial direct support)
Undergraduate Students:	Asma Al-Rawi (directly supported)
	Dana Cristea (5/06-8/06) REU summer student
	Greg Johnson (2/04 – 5/05)
	Matt Wood (5/05 – 8/05) Summer student
	Aaron Pung (8/05 - Present)
	Meredith Sharp (8/05 – 12/05)

Publications:

(The publications listed below were also supported in part by the National Science Foundation through a CAREER grant (ECS-0449295).

Published in peer-reviewed journals:

Rajesh Thapa, Kevin O. Knabe, Mohammed Faheem, Ahmer Naweed, Larry Weaver, and Kristan L. Corwin, "Saturated absorption spectroscopy of acetylene gas inside large-core photonic bandgap fiber", Optics Letters, **31**, 2489 (2006).

R. Thapa, K. Knabe, K. L. Corwin, and B. R. Washburn, "Arc fusion splicing of hollow-core photonic bandgap fibers for gas-filled fiber cells," Optics Express, **14**, 9576 (2006).

Published in peer-reviewed conference proceedings:

"Saturated Absorption Spectroscopy of C_2H_2 Inside a Hollow, Large-Core Kagome Photonic Crystal Fiber," K. Knabe, A. Jones, K. L. Corwin, F. Couny, P. S. Light, and F. Benabid, Tech. Dig., Conf. on Lasers and Electro-Optics and Quantum Electronics and Laser Science Conf. (CLEO/QELS), JFA5, OSA, San Jose, CA (2008).

"Significant Carrier Envelope Offset Frequency Linewidth Narrowing in a Prism-based Cr:forsterite Frequency Comb," K. A. Tillman, R. Thapa, B. R. Washburn, and K. L. Corwin, Tech. Dig., Conf. on Lasers and Electro-Optics and Quantum Electronics and Laser Science Conf. (CLEO/QELS), CTuC5, OSA, San Jose, CA (2008).

"Carrier-envelope phase dynamics in a self-referenced prism-based chromium:forsterite frequency comb," Karl A. Tillman, Rajesh Thapa, Brian R. Washburn and Kristan Corwin, Annual meeting of the Lasers for Electro-Optics Society (LEOS), October 2007, Buena Vista, FL (2007).

"Phase-stabilized Prism-based Cr:forsterite Laser Frequency Comb for Absolute Frequency Measurements," R. Thapa, K. A Tillman, A. Naweed, A. Jones, B. R. Washburn and K. L.

Corwin, Tech. Dig., Conf. on Lasers and Electro-Optics and Quantum Electronics and Laser Science Conf. (CLEO/QELS), May 2007, Baltimore, MD (2007).

"Reflected Pump Technique for Saturated Absorption Spectroscopy Inside Photonic Bandgap Fibers," Kevin Knabe, Rajesh Thapa, Brian R. Washburn, and Kristan L. Corwin, Tech. Dig., Conf. on Lasers and Electro-Optics and Quantum Electronics and Laser Science Conf. (CLEO/QELS), May 2007, Baltimore, MD (2007).

"Comparison of Saturated Absorption Spectra of Acetylene Gas Inside Photonic Bandgap Fibers," K. Knabe, R. Thapa, O. L. Weaver, B. R. Washburn, and K. L. Corwin, Symposium on Optical Fiber Measurement, Sept 18, 2006, Boulder, CO (2006).

"Saturated Absorption Signals from Acetylene Gas Inside Photonic Bandgap Fiber," R. Thapa, K. Knabe, A. Naweed, M. Faheem, O. L. Weaver, and K. L. Corwin, Tech. Dig., Conf. on Lasers and Electro-Optics and Quantum Electronics and Laser Science Conf. (CLEO/QELS), May 23-25, 2006, Long Beach, CA (2006).

"Splicing hollow-core photonic bandgap fiber to solid core fiber using an arc fusion splicer," R. Thapa, K. L. Corwin, and B. R. Washburn, Tech. Dig., Conf. on Lasers and Electro-Optics and Quantum Electronics and Laser Science Conf. (CLEO/QELS), May 23-25, 2006, Long Beach, CA (2006).

"Spectral Hole Burning of Acetylene Gas inside a Photonic Bandgap Optical Fiber", Mohammed Faheem, Rajesh Thapa, and Kristan L. Corwin, Tech. Dig., Conf. on Lasers and Electro-Optics and Electro-Optics/Quantum Electronics and Laser Science Conference (CLEO/QELS), May 2005, Baltimore, MD (2005).

Interactions/Transitions:
(see also peer-reviewed conference proceedings)

"Near-IR frequency comb to characterize sub-Doppler spectroscopy of acetylene-filled optical fibers (poster)," K. L. Corwin, K. Knabe, R. Thapa, K. Tillman, A. Jones, and B. R. Washburn, International Conference on Laser Spectrocsopy (ICOLS), June 2007, Telluride, Colorado, USA (2007).

"'Near-IR frequency comb to characterize acetylene-filled fiber-based frequency references (talk), K. L. Corwin, K. Knabe, R. Thapa, K. Tillman, A. Jones, B. R. Washburn, J. W. Nicholson and M. F. Yan", B5, Annual meeting of the APS Division of Atomic Molecular and Optical Physics (DAMOP), June 2007, Calgary, Canada (2007).

"Saturated Absorption Spectroscopy in Acetylene Filled Photonic Bandgap Fibers," K. Knabe, R. Thapa, O.L. Weaver, B.L. Washburn and K.L. Corwin", Frontiers in Optics and Laser Science, Rochester, NY, 2006.

"Doppler-free saturation spectroscopy of acetylene inside a photonic band-gap fiber," R. Thapa, M. Faheem, and K. L. Corwin, poster at APS DAMOP meeting, Lincoln, NE May 2005.

New discoveries, inventions, or patent disclosures:
"Reflected Pump Technique for Saturated Absorption Spectroscopy inside Hollow Photonic Bandgap Fibers," K. Knabe, R. Thapa, B. R. Washburn and K. L. Corwin, Provisional Patent, Submitted to US Patent Office Sept 18, 2006 (2006).

Honors/Awards:
Center for Economic Development, Innovation and Commercialization
Big 12 Rising Star Award, February 2007.
NSF Career Award, February 2005.

Appendix:
Publications are appended in the order listed above. Afterward, the following manuscript is appended, which is in preparation for submission to Applied Optics:
"Reflected Pump Technique for Fiber-based Saturated Absorption Spectroscopy," K. Knabe, R. Thapa, B. R. Washburn, and K. L. Corwin, in preparation for Applied Optics (2008).

Saturated absorption spectroscopy of acetylene gas inside large-core photonic bandgap fiber

Rajesh Thapa, Kevin Knabe, Mohammed Faheem, Ahmer Naweed, Oliver L. Weaver, and Kristan L. Corwin

Department of Physics, Kansas State University, 116 Cardwell Hall, Manhattan, Kansas 66506

Received March 21, 2006; revised May 5, 2006; accepted May 7, 2006; posted May 25, 2006 (Doc. ID 69166); published July 25, 2006

Saturated absorption spectroscopy is performed on the acetylene $\nu_1+\nu_3$ band near 1532 nm inside photonic bandgap fibers of small (~10 μm) and large (~20 μm) core diameters. The observed linewidths are narrower in the 20 μm fiber and vary from 20 to 40 MHz depending on pressure and power. Variations in the background light transmission, attributed by others to surface modes, are significantly reduced in the 20 μm fiber. The optimum signal for use as a frequency reference in a 0.8 m long, 20 μm diameter fiber is found to occur at about 0.5 torr for 30 mW of pump power. The saturation power is found by modeling the propagation and attenuation of light inside the fiber. © 2006 Optical Society of America

OCIS codes: 060.2310, 300.6460, 120.3930, 230.3990.

Acetylene offers an excellent optical frequency standard in the near-infrared spectral region.[1] Portable references of moderate accuracy (~13–130 MHz), developed at the National Institute of Standards and Technology (NIST), are built into commercial devices.[2] Meanwhile, sub-Doppler spectroscopy inside power buildup cavities has led to the measurement of the $^{13}C_2H_2$ $\nu_1+\nu_3$ $P(16)$ line at 1.542 μm in wavelength to uncertainties as small as 1.4 kHz.[3–5] There are many advantages to performing saturation spectroscopy independent of a power buildup cavity,[6] but long interaction lengths and high optical intensities must be maintained.

Hollow, low-loss photonic bandgap (PBG) fiber[7] is a promising medium in which to develop high-accuracy, portable frequency references. Recently PBG fiber has been employed for studies of gas sensors,[8] Raman shifting,[9] Doppler-broadened frequency references,[10] and electromagnetically induced transparency.[11–13] These studies required a single laser beam or a copropagating geometry. In contrast, sub-Doppler saturation spectroscopy requires counterpropagating pump and probe beams, which can lead to spurious interference that appears as a sinusoidal modulation of the background probe light level. Such background oscillations may limit the performance of a frequency reference. Furthermore, mode beating also appears as a background oscillation. Indeed, initial observations of saturated absorption features inside 10 μm core fibers[13–15] reveal large oscillations in the background, even in the all-fiber configuration.[13] In Ref. 15, the peak-to-peak amplitude of this oscillation is about 20% of the input power and is potentially attributed to surface modes.[16]

We observe a factor of 20 improvement in the background oscillations in 20 μm fiber, which greatly improves the suitability of PBG fibers for frequency references. Saturated absorption features inside 20 μm core PBG fibers are measured at a variety of pressures for a pump power of 29 mW (Fig. 1). The central dip in transmitted power is due to the presence of the pump beam, which burns a Bennett hole[17] in the ground-state population of the acetylene molecules. A laser could be locked to this feature and used as a frequency reference. The background oscillations in the 20 μm fiber core have a peak-to-peak amplitude of less than 1% of the transmitted light. The reduction of these oscillations is likely due to reduced mode beating between surface modes and core modes within the larger-core PGB fiber.[16]

The experimental setup used to realize these saturated absorption spectra is shown in Fig. 2. Two PBG fibers from Crystal Fibre A/S with central wavelengths of 1.55 μm were used. The "20 μm fiber" has 19 missing cells, a core diameter of ~20 μm, and 0.78 m length. The "10 μm fiber" has 7 missing cells, a core diameter of ~10 μm, and 0.90 m length. As shown, both ends of the PBG fiber are fed into the vacuum chambers (VC) via either Torr-seal feedthroughs or compression fitting. Acetylene is introduced into both VCs and equilibrates within the fiber in ~0.5–1 h. A diode laser (ECDL) emits ~5 mW, 10% of which is amplified by a fiber amplifier (EDFA) to up to 500 mW; 70% of this power becomes the

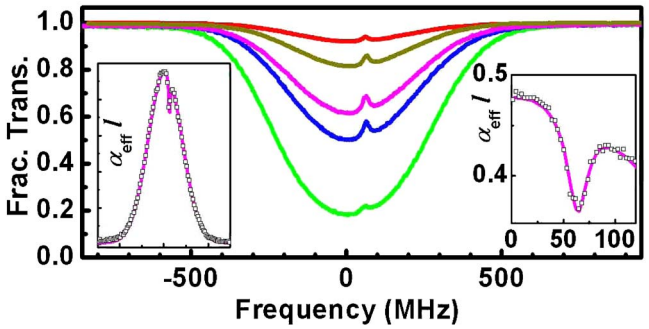

Fig. 1. (Color online) Fractional transmission versus $\Delta\nu$ for the $P(11)$ transition at 1531.6 nm with a pump power of 29 mW incident on the fiber and a counterpropagating probe power of ~1 mW. The $^{12}C_2H_2$ pressure, from top to bottom, was 0.15, 0.26, 0.53, 0.72, and 2.25 torr. Left inset, $\alpha_e(\nu)l$ versus $\Delta\nu$ over the range of ±750 MHz, calculated from the data taken at 0.53 torr (squares) and fitted with Eq. (2) (curve). Right inset, same as left inset, but with expanded axes.

0146-9592/06/162489-3/$15.00

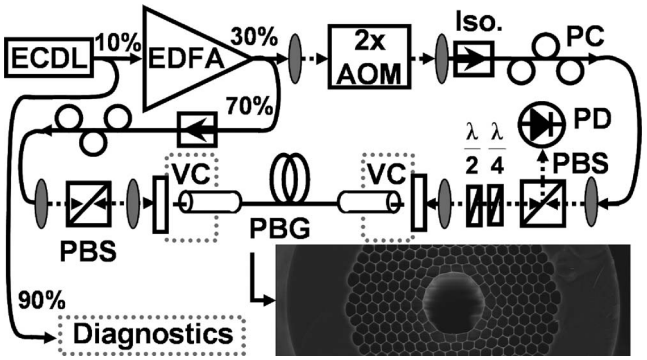

Fig. 2. Schematic of experimental setup. Solid lines indicate optical fiber, and dashed lines indicate free-space optical beams. Aspheric lenses are shown as shaded ovals; the vacuum chambers (VC), indicated schematically, have wedge windows. The PBG image, courtesy of Crystal Fibre A/S, depicts the 20 μm fiber.

pump beam and is coupled into the evacuated PBG fiber after passing an isolator (Iso.), a polarization controller (PC), and a polarizing beam splitter (PBS). The probe beam originates at the EDFA, passes through a double-passed acousto-optic modulator (AOM), an isolator and a PC, and then counterpropagates the pump beam through the PBG fiber. The polarizations of the pump and probe beams do not remain orthogonal inside the PBG fiber. The polarization rotation is corrected by using half-wave and quarter-wave retarders to separate out the probe beam at the PBS. The transmitted probe beam power is detected by a photodetector (PD). The AOM and waveplates minimize the noise due to interference between reflected pump laser light and the probe beam.

The theory of saturated absorption spectroscopy is well known in vapor cells.[17] The propagation of a laser beam with power P_i along the fiber in direction z can be described by $dP_i = -P_i(z)\alpha_i(\nu,z)dz$, with $i = \{u,r\}$ for the case of pump and probe beams, respectively. The pump power is absorbed according to $\alpha_u(\nu,z) = \alpha_D(\nu)/\sqrt{1+S_0(z)}$, where $\alpha_D(\nu) = \alpha_0 \exp[-\Delta\nu^2/(0.36\nu_D^2)]$ is the Doppler-broadened absorption profile, α_0 is the maximum absorption coefficient on resonance, $\Delta\nu$ is the difference between the laser frequency (ν) and the unshifted resonance frequency of the molecules (ν_0), and ν_D is the Doppler width.[17] The resonant saturation parameter $S_0(z) = P_u(z)/P_s$, where the saturation power, P_s, is the power required at frequency ν_0 to pump 1/4 of the ground-state molecules into the excited state.

When the probe beam counterpropagates relative to the pump, with input power $P_r(z=l) = P_{r0}$, the absorption coefficient of the probe beam in terms of S_0 and transition width γ becomes

$$\alpha_r(\nu,z) = \alpha_D(\nu)\left[1 - \frac{S_0(z)\Gamma_s^*(z)}{2\gamma\sqrt{1+S_0(z)}}\frac{(\gamma/2)^2}{\Delta\nu^2 + (\Gamma_s^*(z)/2)^2}\right], \quad (1)$$

where $\Gamma_s^*(z) = \gamma(1+\sqrt{1+S_0(z)})/2$. This is derived according to Ref. 17, but without approximating $S_0 \ll 1$.[18] To simulate the experiment, experimental values of $P_u(z=0)$, $P_r(z=l)$, α_0, P_s, and γ are chosen, and then P_u and P_r are propagated along the fiber numerically. P_s and γ are varied independently until the amplitude and width of the simulated signal match that of the experiment.

To analyze the data, such as those shown in Fig. 1, an effective α is calculated, $\alpha_e(\nu)l = \ln[P_r(\nu,z=0)/P_{r0}(\nu,z=l)]$, and fitted to

$$\alpha_e l = A_g \exp(-2\Delta\nu^2/\sigma^2)\{1 - A_l(w/2)^2/[\Delta\nu_A^2 + (w/2)^2]\}, \quad (2)$$

where $\sigma = 0.849\nu_D$ and $\Delta\nu_A = \Delta\nu - \nu_{AOM}$ includes the shift in the signal due to the AOM. The 10 μm fiber data were fitted with additional terms to account for slope and sinusoidal modulation of the background. Spectra for the 10 μm fiber, not shown, were similar to those in Ref. 15.

The width of the saturation feature (w) varies dramatically between the 10 and 20 μm fibers, as shown in Fig. 3. At comparable pressures, w is consistently greater in the 10 μm fiber over a range of powers, as shown in Fig. 3(a). Fits of the three data sets shown in Fig. 3(a) to $\Gamma_s^*(z=0) = \gamma[1+\sqrt{1+S_0(z=0)}]/2$ yield γ values of 34, 26, and 27 MHz and P_S values of 17, 49, and 43 mW. These fits neglect the significant effect of pump attenuation but offer insight into the physical

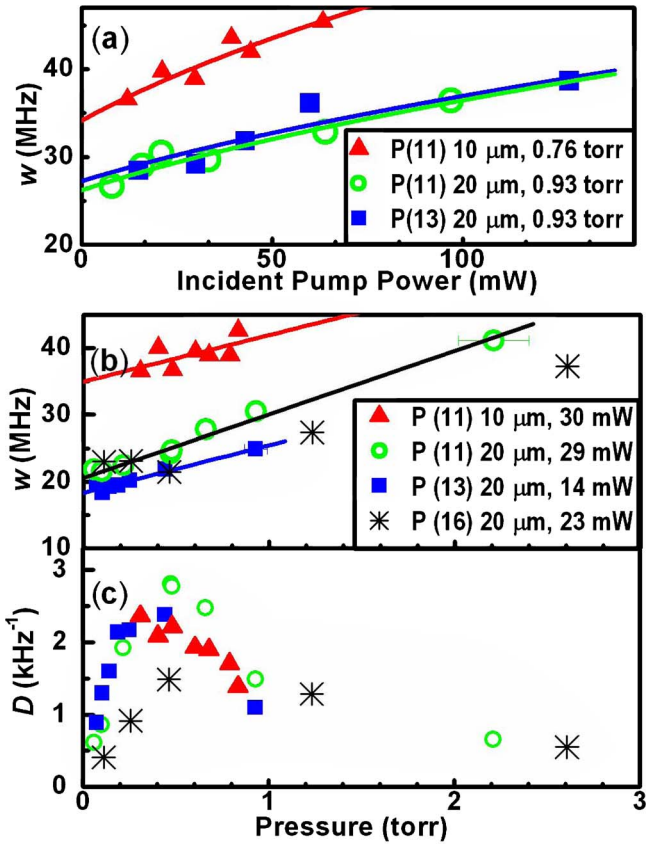

Fig. 3. (Color online) FWHM w versus injected pump power for $P(11)$, $P(13)$, and $P(16)$ transitions in the 10 and 20 μm diameter PBG fibers. (b) Width versus pressure for the same transitions. (c) The frequency discrimination of signals whose widths are shown in (b).

broadening mechanisms. For example, the y intercept, γ, is clearly larger in the case of the 10 μm fiber.

The measured width w is expected to reflect broadening of the natural line width (approximately kilohertz) due to power, pressure, and interaction time between the molecules and the laser beam. The y intercepts of Fig. 3(a) data give the γ of Eq. (1) without power broadening and should reflect pressure broadening and interaction time broadening. Once the pressure broadening of $\sim$11.5 MHz/torr^2 is subtracted, the resulting widths of 16 and 24 MHz in the 20 and 10 μm fiber diameters, respectively, reflect the interaction time broadening, the cause of which may be modeled by wall collisions ($\gamma_{\mathrm{col}}^{\mathrm{wall}}$), as discussed in Benabid *et al.*,[12] or transit time (γ_{tt}). The transit-time-limited width can be approximated as $\gamma_{\mathrm{tt}} = 0.375\nu/r_{1/e}$,[17] where ν is the thermal velocity, which gives 25 and 43 MHz for the same fibers with $1/e$ mode field diameters of 13 and 7.5 μm, respectively.

Figure 3(b) compares w from transitions measured in the 10 and 20 μm fibers as a function of pressure. Again, features in the 10 μm fiber are broader than in the 20 μm fiber. Linear fits to the resulting data give intercepts of 34, 21, 18, and 19 MHz, with slopes of 10, 10, 7, and 7 MHz/torr, respectively (1 torr = 133 Pa). These are smaller than the pressure broadening measured in higher-pressure systems, but the discrepancy may be due to the reduction in power broadening at higher pressure, due to stronger attenuation of the pump beam.

A figure of merit for a frequency reference, "discrimination" (D), can be calculated based on the fractional change in optical power transmission divided by the transition width. The value of D is thus proportional to the derivative signal obtained from modulation spectroscopy, which would be required in order to peak-lock a laser to the saturated absorption feature. We define $D = \{\exp(-A_G) - \exp[-A_G(1 - A_L)]\}/w$. Figure 3(c) shows D, the figure of merit for the frequency discrimination of the signals. For comparison, the Doppler-broadened resonances of Benabid *et al.*[10] have a D of about 1 kHz^{-1}, while the cavity-based standards have $D = 40$ kHz^{-1}. Thus the discrimination of PBG fiber-based references does not yet rival cavity-based standards, but is clearly superior to Doppler-broadened lines. The optimum conditions for operating a frequency reference at a given input pump power inside PBG fiber can be deduced from this plot. In Fig. 3(c) the $P(11)$ data were taken at a higher pump power than the $P(13)$ and therefore exhibit a higher value of D. The optimum pressure is expected to depend nearly inversely on fiber length for long fibers.

Numerical modeling by two methods gives values for P_s. The first method, based on measured attenuation of the pump beam only, gives 22 ± 4 mW, in agreement with Henningsen *et al.*[15] and using the same approach. The simulations described above yield $P_S = 34 \pm 4$ mW. Error in both cases is primarily systematic and is found by taking the standard deviation of $\sim$20 measurements. The discrepancy between the two approaches remains unresolved.

We have investigated saturation spectroscopy inside large-core PBG fiber and observed narrower transitions and much cleaner signals than those observed in smaller-core PBG fibers.

We thank Kurt Vogel for suggesting the AOM, Greg Johnson, Mike Wells and the J. R. Macdonald Lab staff for help building the experiment, and Sarah Gilbert, Dirk Müller, Bill Swann, and Brian Washburn for helpful discussions. We gratefully acknowledge funding from the Air Force Office of Scientific Research, the National Science Foundation CAREER and EPSCoR programs, and Kansas Technology Enterprise Corporation. K. Corwin's email address is corwin@phys.ksu.edu.

References

1. T. J. Quinn, Metrologia **40**, 103 (2003).
2. W. C. Swarnn and S. L. Gilbert, J. Opt. Soc. Am. B **17**, 1263 (2000).
3. C. S. Edwards, H. S. Margolis, G. P. Barwood, S. N. Lea, P. Gill, and W. R. C. Rowley, Appl. Phys. B **80**, 977 (2005).
4. J. Jiang, A. Onae, H. Matsumoto, and F. L. Hong, Opt. Express **13**, 1958 (2005).
5. A. Czajkowski, J. E. Bernard, A. A. Madej, and R. S. Windeler, Appl. Phys. B **79**, 45 (2004).
6. A. Onae, K. Okumura, Y. Miki, T. Kurosawa, E. Sakuma, J. Yoda, and K. Nakagawa, Opt. Commun. **142**, 41 (1997).
7. R. F. Cregari, B. J. Mangan, J. C. Knight, T. A. Birks, P. S. Russell, P. J. Roberts, and D. C. Allan, Science **285**, 1537 (1999).
8. T. Ritari, J. Tuominen, H. Ludvigsen, J. C. Petersen, T. Sørensen, T. P. Hansen, and H. R. Simonsen, Opt. Express **12**, 4081 (2004).
9. F. Benabid, G. Bouwmans, J. C. Knight, P. S. J. Russell, and F. Couny, Phys. Rev. Lett. **93**, 123903 (2004).
10. F. Benabid, F. Couny, J. C. Knight, T. A. Birks, and P. S. J. Russell, Nature **434**, 488 (2005).
11. S. Ghosh, J. E. Sharping, D. G. Ouzounov, and A. L. Gaeta, Phys. Rev. Lett. **94**, 093902 (2005).
12. F. Benabid, P. S. Light, F. Couny, and P. S. Russell, Opt. Express **13**, 5694 (2005).
13. P. S. Light, F. Couny, F. Benabid, and P. S. J. Russell, in *Proceeding of the 31st European Conference on Optical Communication (ECOC 2005)* (IEE, 2005), Vol. 6, p. 59.
14. M. Faheem, R. Thapa, and K. L. Corwin, presented at *Conference on Lasers and Electro-optics (CLEO) 2005*, Baltimore, Md., May 21–26, 2005.
15. J. Henningsen, J. Hald, and J. C. Petersen, Opt. Express **13**, 10475 (2005).
16. J. A. West, C. M. Smith, N. F. Borrelli, D. C. Allan, and K. W. Koch, Opt. Express **12**, 1485 (2004).
17. W. Demtröder, *Laser Spectroscopy* (Springer, 1996).
18. R. Thapa, "Doppler-free spectroscopy of acetylene in near infrared spectral region inside photonic band gap fiber," M.S. thesis (Department of Physics, Kansas State University, 2005), http://dspace.cns.ksu.edu:4001/dspace/handle/2097/133.

Arc fusion splicing of hollow-core photonic bandgap fibers for gas-filled fiber cells

R. Thapa, K. Knabe, K. L. Corwin, and B. R. Washburn
Kansas State University, Dept. of Physics, 116 Cardwell Hall, Manhattan, KS 66506
washburn@phys.ksu.edu

Abstract: The difficulty of fusion splicing hollow-core photonic bandgap fiber (PBGF) to conventional step index single mode fiber (SMF) has severely limited the implementation of PBGFs. To make PBGFs more functional we have developed a method for splicing a hollow-core PBGF to a SMF using a commercial arc splicer. A repeatable, robust, low-loss splice between the PBGF and SMF is demonstrated. By filling one end of the PBGF spliced to SMF with acetylene gas and performing saturation spectroscopy, we determine that this splice is useful for a PBGF cell.

OCIS codes: (060.4510) Optical communications; (120.3930) Metrological Instrumentation; (300.1030) Absorption; (230.3990) Microstructure devices;

References and links

1. F. Benabid, P. S. Light, F. Couny, and P. S. J. Russell, "Electromagnetically-induced transparency grid in acetylene-filled hollow-core PCF," Opt. Express **13**, 5694-5703 (2005).
2. S. Ghosh, J. E. Sharping, D. G. Ouzounov, and A. L. Gaeta, "Resonant optical interactions with molecules confined in photonic band-gap fibers," Phys. Rev. Lett. **94**, 093902-1 (2005).
3. J. Henningsen, J. Hald, and J. C. Peterson, "Saturated absorption in acetylene and hydrogen cyanide in hollow-core photonic bandgap fibers," Opt. Express **13**, 10475-10482 (2005).
4. R. Thapa, K. Knabe, M. Faheem, A. Naweed, O. L. Weaver, and K. L. Corwin, "Saturated absorption spectroscopy of acetylene gas inside large-core photonic bandgap fiber," Opt. Lett. **31**, 2489-2491 (2006).
5. T. Ritari, J. Tuominen, H. Ludvigsen, J. C. Petersen, T. Sørensen, T. P. Hansen, and J. C. Simonsen, "Gas sensing using air-guiding photonic bandgap fibers," Opt. Express **12**, 4080-4087 (2004).
6. F. Benabid, F. Couny, J. C. Knight, T. A. Birks, and P. S. J. Russell, "Compact, stable and efficient all-fibre gas cells using hollow-core photonic crystal fibres," Nature **434**, 488-491 (2005).
7. T. Ritari, G. Genty, and H. Ludvigsen, "Supercontinuum and gas cell in a single microstructured fiber cell," Opt. Lett. **30**, 3380-3382 (2005).
8. A. Yablon, *Optical fiber fusion splicing* (Springer, Heidelberg, 2005).
9. P. S. Light, F. Couny, and F. Benabid, "Low optical insertion-loss and vacuum-pressure all-fiber acetylene cell based on hollow core PCF," Opt. Lett. **31**, 2538-2540 (2006).
10. P. J. Bennett, T. M. Monro, and D. J. Richardson, "Toward practical holey fiber technology: fabrication, splicing, modeling, and characterization," Opt. Lett. **24**, 1203-1205 (1999).
11. B. Bourliaguet, C. Paré, F. Émond, A. Croteau, A. Proulx, and R. Vallée, "Microstructured fiber splicing," Opt. Express **11**, 3412-3417 (2003)..
12. Crystal Fibre A/S, http://www.crystal-fibre.com/support/faq.shtm.
13. L. Xiao, W. Jin, M. S. Demokan, H. L. Ho, Y. L. Hoo, and C. Zhao, "Fabrication of selective injection microstructured optical fibers with a conventional fusion splicer," Opt. Express **13**, 9014-9022 (2005).
14. Corning SMF-28e optical fiber product information, http://www.corning.com/opticalfiber/.
15. Crystal Fibre A/S HC19-1550-01 product information, http://www.crystal-fibre.com.
16. Crystal Fibre A/S HC-1550-02 product information, http://www.crystal-fibre.com.
17. J. H. Chong and M. K. Rao, "Development of a system for laser splicing photonic crystal fiber," Opt. Express **11**, 1365-1370 (2003).
18. D. Gloge, "Weakly guiding fibers," Appl. Opt. **10**, 2252-8 (1971).
19. C. R. Pollack, *Fundamentals of Optoelectronics* (Irwin, Chicago, 1995), Chap. 11.
20. G.-i. Kweon and I.-S. Park, "Splicing losses between dissimilar optical waveguides," J. of Lightwave Technol. **17**, 690-703 (1999).

1. Introduction

Photonic bandgap fibers (PBGF) are optical waveguides that will serve as a key technology to enable future advances in frequency metrology, spectroscopy, and quantum optics. A PBGF is a low-loss waveguide whose hollow core can be filled with a fluid, allowing light to interact with the fluid while being guided by the PBGF geometry. Recently, much progress has been made using gas-filled PBGF, including the observation of resonant interactions and electromagnetically-induced transparency in acetylene-filled fibers, which has important applications toward all-optical fiber communications [1, 2]. Saturation spectroscopy, for higher-accuracy portable optical frequency references, has also been demonstrated [3, 4]. Even linear interactions are significantly enhanced in PBGFs, resulting in the development of gas sensors [5] and Doppler- and pressure-broadened frequency references [6, 7].

Splices between microstructured fibers and step index single-mode fibers (SMF) are difficult to create, because the air holes in the fiber tend to collapse at the high temperatures required to form a strong splice (see Ref. [8] and references therein). Splicing solid-core microstructured optical fibers to SMF is typically accomplished with filament splicers [6, 9, 10], but has also been demonstrated using an arc splicer [11]. Indeed, splicing SMF to hollow-core PBGF is even more difficult due to the presence of the large guiding hole, and this difficulty limits the use of these fibers in laboratory experiments or in commercial products. However, successful splices between hollow-core PBGF and SMF have been made using a filament-based fusion splicer, and are commercially available [12]. Furthermore, arc splicers have been used to systematically investigate the collapse of air holes in PBGF for selective injection [13], but until now, no low-loss, robust splices have been made with the relatively inexpensive and ubiquitous arc fusion splicer.

Many applications of PBGF require the fabrication of a PBGF cell, in which a length of PGBF is filled with a gas or liquid and spliced to solid-core single-mode fiber on each end. This cell is doubly difficult to produce since 1) two low-loss splices between the SMF and PBGF fiber must be made and 2) at least one splice must be made while keeping the gas in the PBGF microstructures. Such PBGF cells have been created [6, 7, 9] where the first splice between the PBGF and SMF is made in air, while the second splice to SMF must be made in a gas atmosphere. In fact, PBGF have been sealed after being filled by acetylene gas [6], but this technique relies on the use of an expensive, filament-based fusion splicer. Another clever method of making gas-filled PBGF cells involves splicing the PBGF to SMF in a helium and acetylene gas purge using a filament splicer [9]. The helium diffuses from the PBGF, leaving only high purity acetylene in the cell. Nevertheless, a simple recipe for splicing PBGF to SMF using a conventional arc fusion splicer has until now been lacking. Here we demonstrate a repeatable, robust, low-loss splice between a hollow-core PBGF and SMF. The performance of this fiber compares favorably with a commercially made spliced fiber.

2. Fusion splicing hollow-core PBGF to SMF

2.1 Specific fibers used in this study

Two types of hollow-core PBGF, both purchased from Crystal Fibre A/S, are discussed in this study. The PBGFs were spliced to Corning® SMF-28e® SMF using an Ericsson FSU-995 electric arc fusion splicer. The first PBGF, part number HC-1550-02, has a hole diameter of 10.9 μm and a mode overlap of >90 % with the SMF. The second PBGF, part number HC19-1550-01, has a hole diameter of 20 μm. The significant fiber parameters are listed in Table 1.

Table 1. Fiber Parameters for the PBGF and the Single-Mode Fiber

Fiber Name	Core diameter	Mode-field diameter	Numerical Aperture	Hole Separation Λ
HC-1550-02	10.9 μm	7.5 μm[†]	0.12[†]	3.8
HC19-1550-01	20 μm	13 μm[‡]	0.13[‡]	3.9
SMF-28e	8.2 μm	10.4 μm[†]	0.14	--

[†]Values given at 1550 nm [14]. [‡]Values given at 1570 nm [15, 16].

2.2 Splicing procedure using an electric arc splicer

Filament splicers are generally preferred for fusion splicing PBGFs since they heat the fiber more slowly and uniformly. Our goal, which is motivated largely by the cost and popularity of arc fusion splicers, is to mimic this performance with a more common electric arc fusion splicer. One difficulty in splicing hollow-core PBGF is avoiding the collapse of the microstructures, because temperatures that are high enough to form a strong splice also allow the glass to flow. Splicing PBGF is particularly difficult using an electric arc splicer because the fibers are heated very rapidly during the arc. Thus, we have developed a multi-step splice procedure involving a short, high current arc followed by a long, low current arc. In general, the amount of current used in this process is less than that of a conventional splicing procedure.

The geometry of the fusion splicer is illustrated in Fig. 1. There are two parameters that define the distance of the fibers from the electric arc and from each other. The first parameter called "gap" measures the distance between the two fibers. Zero gap, which occurs at a position called the "touch point" indicates that the fibers are butt-coupled. Negative gaps, here called "overlap", indicate that the fibers are pushed further together than they were when butt-coupled. The second parameter called "offset" indicates the displacement of the touch point from the electrode axis. In all splices, the fibers are prepared by mechanically stripping the coating away from the last ~2.5 cm of fiber, and cleaved using a Fujikura CT-04B cleaver.

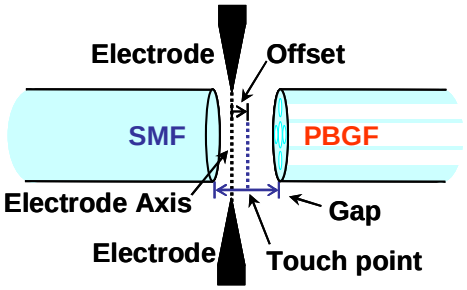

Fig. 1. The fusion splicer geometry. Two variable parameters, gap/overlap and offset, determine the position of the fibers with respect to the electrode axis.

The optimum procedure for splicing PBGF to SMF was developed by attempting more than twenty splices with a wide range of splice parameters. The resulting optimized program for splicing SMF-28e® to the 10.9 μm PBGF HC-1550-02 is as follows. The splicing program first aligns the fibers and produces a short burst of current (pre-fuse) to remove any contamination present in the fiber end. This pre-fuse also removes any moisture in the microstructures that will cause the splice to be fragile. Next, the fibers are briefly butt-coupled at the touch point, and a gap of +10 μm is made. The offset is set to 260, placing the electrodes roughly 5 μm closer to the SMF than the PBGF (as determined using Ref. [13]). The butt-coupled loss from the SMF to the 10.9 μm PBGF is typically 1.0 dB. The nonzero offset is a critical parameter in the splicing since it ensures that the SMF is heated more strongly than the PBGF, to prevent the collapse of the air holes [17]. Fusion current 1 is set to 10 mA and applied for 0.2 s, which softens both fiber ends and prepares the fibers to be overlapped and fused together upon physical contact in the next process. Care must be taken while choosing this current level because a low arc current leads to a mechanical deformation during the overlapping stage, while a high current causes a change in the glass geometry resulting in a poor quality splice. If fusion current 1 is reduced from the optimum splicing condition of 10 mA to 9 mA for the same duration (0.2 s), the resulting splice loss is approximately the same in both cases, but the mechanical strength of the splice is greatly reduced. If for a constant fusion current 1 (10 mA) the time is increased beyond 0.2 s, the PBGF end deforms or collapses completely under surface tension, forming a spherical end.

Fusion current 2 starts when the fiber ends actually touch and press together in order to overlap and to fuse. During this phase, the current is reduced to 7 mA for 12 s while the fibers are pushed together to a negative gap, or overlap, of 10 µm. Increasing the overlap at optimum arc current to 15 µm gives a better mechanical strength (the splice breaking when bent at a radius of 1.5 cm compared to 1.7 cm) with comparable or slightly higher splice loss, while a smaller overlap of 5 µm gives a splice with comparable loss but which is extremely fragile. To complete the procedure the fusion current 3 is set to 6.5 mA for 3 s, while the splice anneals. Figure 2 illustrates the loss with respect to the butt-coupled transmission measured during the splicing procedure.

The splice routine was altered for splicing the SMF-28e® to the 20 µm PBGF HC19-1550-01. The only significant change in the program was the increase in the overlap from 10 µm to 15 µm in order to compensate for the larger hole diameter.

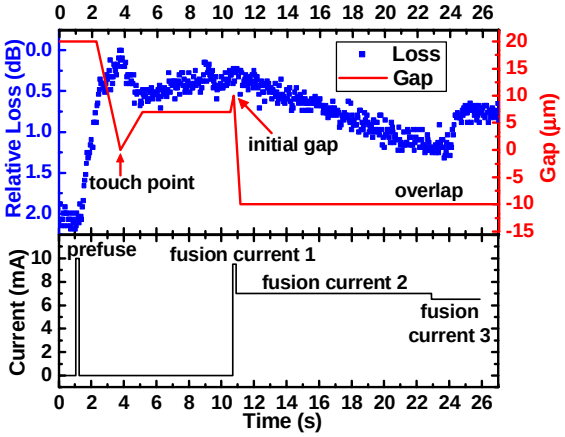

Splice Parameters		
Fiber Type	HC-1550-02	HC19-1550-01
Prefuse time	0.2 s	0.2 s
Prefuse current	10 mA	10 mA
Gap	10 µm	10 µm
Overlap	10 µm (9 µm)	15 µm
Fusion time 1	0.2 s	0.2 s
Fusion current 1	10 mA (9 mA)	10 mA
Fusion time 2	12 s (8 s)	12 s
Fusion current 2	7 mA (6.9 mA)	7 mA
Fusion time 3	3 s	3 s
Fusion current 3	6.5 mA (6.3 mA)	6.5 mA
Offset	260	260

Fig. 2. The relative loss with respect to the butt-coupled transmission from the SMF to the 10.9 µm PBGF during the fusion procedure. The gap curve is estimated from the splice parameters, the Ericsson FSU-995-FA fusion splicer manual, and the relative loss curve. The values in parenthesis indicate altered parameters for new electrodes.

2.3 Splice loss between SMF and PBGF

The splice loss is determined directly by measuring the transmission of a 1534 nm laser source through the splice, in both directions, using the following procedure. To measure the loss from SMF to PBGF, first the cw laser light is injected into the SMF fiber and the output power is measured. Then the SMF is spliced to the PBGF and the output power from the PBGF is measured. To measure the splice loss from the PBGF to SMF, the other end of the PBGF is subsequently spliced to another SMF and the output power is again measured.

The measured loss for splices of SMF to both the 20 µm and the 10.9 µm PBGFs are listed in Table 2. For both splices, the most unique feature is the non-reciprocity of the splice loss: the splice loss as measured from the SMF to PBGF is different from that measured in the opposite direction from the PBGF to SMF. In the 20 µm HC19-1550-01 fiber, splice loss from SMF to PBGF varies from 0.3 dB to 0.5 dB whereas splice loss from PBGF to SMF is more than 2 dB. The splice loss non-reciprocity is less prominent in 10.9 µm PBGF.

To verify the reproducibility of the procedure we made a series of splices measuring the loss in one direction. Four 20 µm SMF/PBGF splices were made on over the course of three weeks using the above recipe that had an average splice loss of 0.42 dB with a standard deviation of 0.09 dB. Also, five 10 µm SMF/PBGF splices were made with an average loss of 1.74 dB with a standard deviation of 0.19 dB. These results determine the range of values in Table 2. As further evidence for the splice reproducibility, a series of consecutive splices were made eight months after the development of the procedure. We had to replace the

splicer's electrodes since our initial reproducibility study above, but after a slight optimization the recipe worked well. The modified parameters for new electrodes are listed in Fig. 2. For the 10 μm fiber, we performed five SMF/PBGF splices in quick succession, taking about 20 minutes per splice, using the same splice parameters. Each splice was successful on the first attempt with the loss values of 1.8 dB, 1.5 dB, 1.8 dB, 1.9 dB, and 1.7 dB for the five splices.

Table 2. Measured Non-Reciprocal Splice Loss between PBGF to SMF

Splice Type	PBGF Core diameter	Loss from SMF to PBGF	Loss from PBGF to SMF
SMF-28e/HC-1550-02	10.9 μm	1.5-2.0 dB	2.6-3.0 dB
SMF-28e/HC19-1550-01	20 μm	0.3-0.5 dB	> 2.0 dB[†]

[†]Value was determined indirectly from the transmission through 20 μm PBGF cells.

Unfortunately the splice loss depends on the orientation of the PBGF, which we attribute to the multimode nature of the PBGF. To see this effect, fiber cells of both 10.9 and 20 μm fiber were made and the splices were fixed to a table. For example when one 20 μm PBGF cell was moved randomly, the loss varied erratically from 2.2 to 6.0 dB through the entire cell. For a 10.9 μm fiber cell a smaller change from 4.2 to 5.3 dB was observed.

A physical explanation of the observed splice loss is difficult due in part to the complicated mode structure of the PBGF. This measured splice loss can be explained rigorously by computing the overlap integral between the PBGF and SMF modes. Unfortunately the determination of this integral is impossible since the amount of energy in each guided mode is typically unknown [8]. Also, it is difficult to compute the number of modes of the PBGF without resorting to a numerical method for computing the modes.

Qualitative arguments based on the theory of step-index fibers [18] can be used to explain the observed loss and the non-reciprocal loss. An estimate of the minimum loss can be computed from the mode overlap of two Gaussian profiles with mode field radii r_1 and r_2. This overlap integral (assuming no axial mismatch) can be evaluated to give the minimum splice loss in dB as [19]

$$10Log_{10}\left(4r_1^2r_2^2\left(r_1^2+r_2^2\right)^{-2}\right). \quad (1)$$

Using this equation the minimum loss for the 10 μm PBGF to SMF splice is 0.45 dB while the minimum splice loss for the 20 μm PBGF to SMF splice is 0.21 dB. Interestingly, this approximation predicts that the 20 μm PBGF will have a lower minimum splice loss than the 10.9 μm PBGF, which is indeed observed.

The crude splice loss approximation given in Eq. (1) based on mode-field radii does not predict the non-reciprocal loss. However, this non-reciprocal loss can be explained in terms of mode mismatching between multimode waveguides [20]. The problem here is similar to the coupling between a SMF and a multimode fiber (MMF) at a given optical wavelength. For this scenario, there is a general rule that the loss from a small core fiber to a large core fiber be smaller than the loss in the other direction. In the case of coupling from SMF to MMF the loss is expected to be small [8]. The mode field radius of the SMF is smaller than that of the MMF so it can easily couple to the lowest order modes of the MMF. The opposite behavior occurs when coupling from the MMF to SMF. Here, higher order modes will be excited in the MMF that will not couple well to the SMF. From these arguments, it is expected that a larger asymmetry in splice loss will occur with a larger number of modes in the PBGF. Due to its larger diameter, the 20 μm PBGF supports more modes (~ 10 modes) than the 10.9 μm fiber (~ 1-3 modes). Thus the HC19-1550-01/SMF-28e splice should exhibit a more prominent non-reciprocal splice loss than the 10 μm PBGF. As described above, the 20 μm PBGF to SMF loss was much more susceptible to fiber positioning than the

10.9 μm PBGF to SMF loss. The observation is consistent with the 20 μm PBGF containing more modes than the 10.9 μm PBGF.

Figure 3 shows a micrograph of the HC-1550-02/SMF-28e splice. In general the splices are mechanically strong and can be bent to a ~1.5 cm circular radius before breaking.

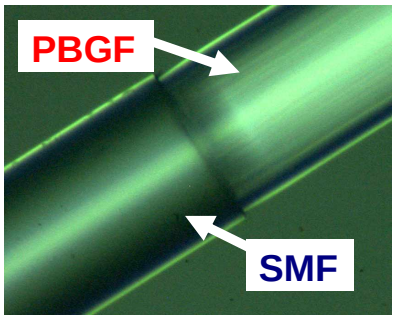

Fig. 3. A micrograph showing the splice between the SMF and 10.9 μm PBGF. Picture courtesy of the GaN Group in the Kansas State University Physics Department.

3. PBGF-SMF splice for a gas-filled PBGF cell

3.1 Absorption spectroscopy

One important application of PBGF-SMF splices is in the creation of gas-filled PBGF cells. Saturated absorption spectroscopy on such cells is a promising technology for portable optical frequency references, but sensitive to the splice quality. This sensitivity arises because light reflected from both splices can form a standing wave as in a Fabry-Perot cavity, and thus the fiber cell transmission depends periodically on optical frequency. This frequency-dependent "background" creates a shift in the apparent line center of the absorption feature of the reference gas, such as acetylene, and thus degrades the performance of the frequency reference.

The splices will be useful in a PBGF cell, as demonstrated using saturation spectroscopy on acetylene inside PBGF that is spliced to SMF fiber. Several different fibers and splices are then compared. The experimental set-up is shown in Fig. 4, and is similar to that of Ref. [4]. Here, a PBGF spliced to SMF is evacuated by pumping with a mechanical roughing pump on the PBGF's open end in a vacuum chamber. The fiber is evacuated to ~15 mtorr over 12 hours. Then the vacuum chamber and PBGF are filled with acetylene gas to a pressure of 0.9 torr. Absorption spectroscopy on the gas in the PBGF reveals a strong absorption feature. Light from a ~1531 nm tunable diode laser is amplified by an erbium-doped fiber amplifier and split to produce a probe (~1 mW) and pump (~30 mW). The probe beam passes through a double-passed acousto-optic modulator, an isolator, and a polarization controller, and then counter-propagates the pump beam through the PBGF. The transmitted probe beam power is detected by a photodetector as the diode laser frequency scans across the absorption feature. The laser is swept eight times across the signal, and the eight traces are averaged on an oscilloscope.

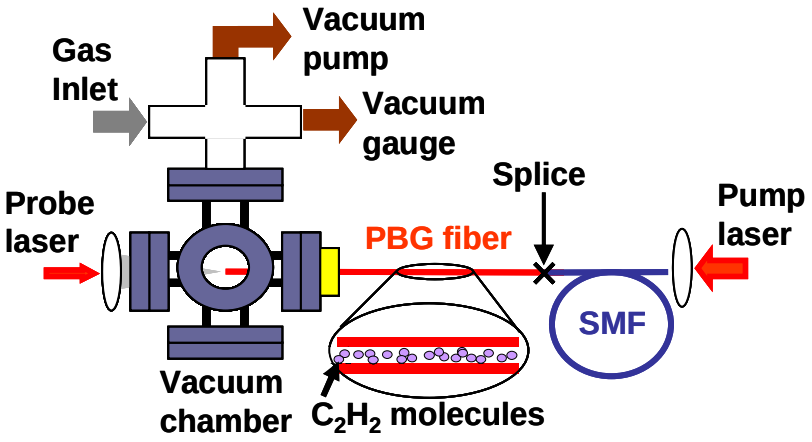

Fig. 4. Chamber used to evacuate and fill the PBGF with acetylene gas for saturated absorption spectroscopy.

Saturated absorption spectra are shown in Fig. 5; here the spectra between different 10.9 µm and 20 µm fibers are compared. Figure 5(a) compares three 10.9 µm PBGFs: Fiber 1 is 0.78 m long spliced to SMF with an arc splicer; Fiber 2 is 2.0 m long spliced to SMF with a commercial filament fusion splicer (spliced and purchased from Crystal Fibre) [12]; and Fiber 3 is 0.9 m long unspliced. Figure 5(b) compares two 20 µm PBGFs: Fiber 4 is 0.4 m long spliced to SMF with an arc splicer as described above, and Fiber 5 is 0.78 m long unspliced. Two vacuum chambers were used to perform the saturation spectroscopy on the unspliced PBGFs [4]. The 10.9 µm fibers exhibit some dependence of transmission with frequency, with similar interference fringe contrast ratios of ~5%-10%. In contrast, the 20 µm fiber splices exhibit much smaller interference fringe contrast ratios of less than 0.5%. Thus these fringes are not thought to arise from the splice, but rather to be intrinsic to the fiber, due for example to mode beating associated with the excitation of surface modes. In both cases the splice does not significantly impact the quality of the saturated absorption feature. Of course, a fiber cell requires two splices, one of which can be made by the above method. Further investigations will be required to characterize and minimize the impact of reflections from a second splice on the signal quality of the cell.

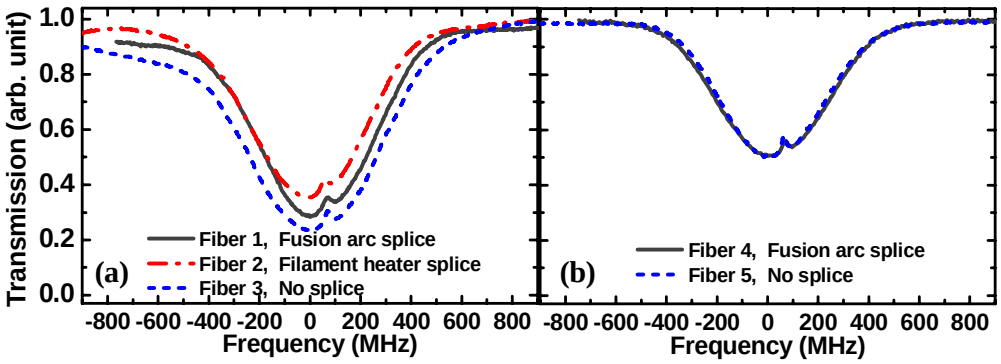

Fig. 5. Saturated absorption spectra in (a) 10.9 µm and (b) 20 µm diameter PBGFs. Fiber 1 is 0.78 m long, spliced to SMF using a conventional arc splicer using the technique described in this paper. The P(11) spectrum was taken at 29 mW and 0.9 torr. Fiber 2 is 2.0 m long, spliced to SMF by Crystal Fibre A/S using a filament heating splicer, and its spectrum is taken of the weaker P(12) transition at 17 mW and 0.8 torr. Fiber 3 is the unspliced 10.9 µm fiber of 0.9 m long, the P(11) spectrum was taken at 30 mW of pump power at 0.6 torr. Fiber 4 is 0.4 m long, spliced with an arc splicer to SMF, the P(11) spectrum was taken at 34 mW and 0.9 torr. Fiber 5 is unspliced fiber 0.78 m long, and the P(11) spectrum was taken at 29 mW of pump power at 0.7 torr.

4. Summary

We have demonstrated a repeatable, low-loss fusion splice between PBGF and SMF using a commercial arc fusion splicer whose loss compares well to splices made with a filament fusion splicer. The minimum observed splice loss is consistent with expected losses due to mode field mismatch, while the asymmetry is attributed to the multimode nature of the PBGF. Furthermore, the splice did not degrade the quality of saturated absorption spectra when used at one end of a gas-filled fiber cell. Future work will involve sealing the PBGF with a second low loss splice in an acetylene atmosphere while filling the PBGF, using a CO_2 laser.

Acknowledgments

We thank the James R. Macdonald Laboratory staff for construction of the vacuum chambers, and Andrew Jones and Larry Weaver for helpful discussions. This material is based upon work supported by the Air Force Office of Scientific Research under contract No. FA9950-05-1-0304 and the National Science Foundation under Grant No. 0449295.

Saturated Absorption Spectroscopy of C_2H_2 Inside a Hollow, Large-Core Kagome Photonic Crystal Fiber

Kevin Knabe, Andrew Jones, and Kristan L. Corwin

Kansas State University, 116 Cardwell Hall, Manhattan, KS 66506.USA
corwin@phys.ksu.edu

Francois Couny, Philip S. Light, and Fetah Benabid

Centre for Photonics and Photonic Materials, Department of Physics,University of Bath, Claverton Down, Bath BA2 7AY, United Kingdom

Abstract: Saturated absorption spectroscopy in acetylene-filled, 19-cell kagome-structured hollow core photonic crystal fiber is investigated. The large core size of ~70 µm allows for narrow sub-Doppler features, and the wavelength-insensitive transmission is suitable for frequency measurements.

OCIS codes: (300.6460) Spectroscopy, saturation; (060.2310) Fiber optics

1. Introduction

Hollow-core photonic crystal fibers (HC-PCFs) based on photonic bandgap (PBG) and kagome structures facilitate nonlinear optical interactions with molecular gases and alkali vapors. The portable, robust nature of such fibers holds promise for portable frequency references in the near IR. Saturated absorption spectroscopy (SAS) and copropagating resonant interactions have been demonstrated in PBG fibers filled with acetylene [1-3]. Widths are limited by the interaction time (between the molecules and the laser before hitting the cell walls) to greater than 20 MHz. By selecting the low-velocity atoms, widths of 15 MHz FWHM have been observed [3]. Kagome fiber [4], which was used to observe SAS in Rb [5], possesses a lattice with a much larger unit cell and consequently offers larger core sizes. Furthermore, because of the intrinsic nature of the optical guidance mechanism in these fibers [4], the coupling between the core and the cladding silica modes is dramatically reduced, resulting in a more frequency insensitive transmission than in the PBG fiber. Here we have observed saturated absorption spectra in 19-cell kagome fiber with a core diameter of ~70 µm, and investigated the dependence on pressure and power. We have also used frequency modulation (FM) spectroscopy to lock a diode laser to the absorption feature [6].

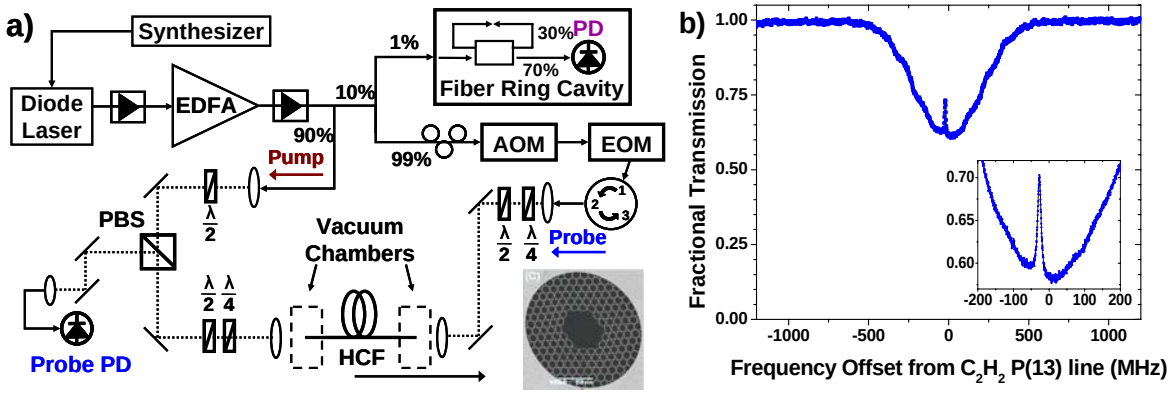

Figure 1a. Saturated absorption spectroscopy setup with SEM image of 19-cell, ~70 µm core diameter kagome HCF from Ref. [4]. Diode laser (DL), erbium doped fiber amplifier (EDFA), photo-detector (PD), polarizing beam splitter (PBS), acousto-optic modulator (AOM), and electro-optic modulator (EOM). 1b. Fractional transmission of the P(13) line in C_2H_2 using a synthesizer to drive the PZT to scan the laser frequency. The inset shows the reduction in noise when the synthesizer drives the diode current (at a frequency higher than the PZT scan). The acetylene pressure inside the fiber was 175 mT, and the pump power was 140 mW exiting the fiber.

2. Saturated Absorption Spectroscopy

The experimental setup for SAS on C_2H_2-filled kagome fibers is shown in Fig. 1a, and a similar setup is explained in Ref [2]. Spectra were recorded at several different acetylene pressures and optical pump powers. These spectra are converted from the recorded transmission (Fig.1b) to the dimensionless absorbance times length as described in Ref. [2]. The FWHMs of the sub-Doppler absorbance feature, w_l, are plotted below as both a function of pressure and of power. Sub-Doppler widths inside the kagome fiber are an expected 2-3 times smaller than those observed in PBG fiber (of the same length and optical power), due to the increased molecular interaction time.

The discrimination (D) is a measure of the slope of the sub-Doppler feature on the fractional transmission signal, and is maximized near the optimum pressure for laser locking conditions to achieve diode laser stabilization. Maximum D values observed inside kagome fiber are ~2 times larger than those observed inside PBG fibers at comparable powers.

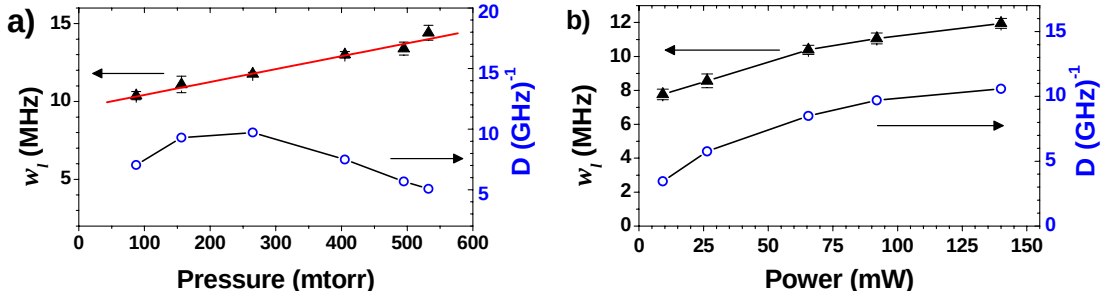

Figure 2a. Sub-Doppler FWHM width, w_l, and discrimination, D, versus pressure. The optical pump power was 92 mW exiting the 1.4 m kagome fiber. The fit line for w_l has a slope of 8.2 MHz/torr, and an 0-pressure intercept of 9.6 MHz. 2b. Sub-Doppler width, w_l, and discrimination, D, versus power. The internal acetylene pressure was 175 mtorr inside the 1.4 m fiber. The graph extrapolates to 7.3 MHz when power = 0.

3. FM Spectroscopy

To detect the SAS feature with high fidelity, FM spectroscopy techniques are employed [6]. Sidebands spaced by f_m = 20 MHz are added to the probe laser with an EOM. The probe PD in Fig. 1 has also been replaced with a fast PD (detector response > f_m) in Fig. 3. The response of the fast PD is then mixed with a synthesizer modulating at f_m with adjustable phase. Because the signal of interest occurs near DC, the output from the mixer (Fig. 3) is low-pass filtered. This signal is then sent to a side-locking servo circuit, which is in turn used to feedback to the current in the laser. The laser has been locked to better than 200 kHz pk-pk as measured in-loop. Studies are planned to measure the absolute frequency of the locked laser.

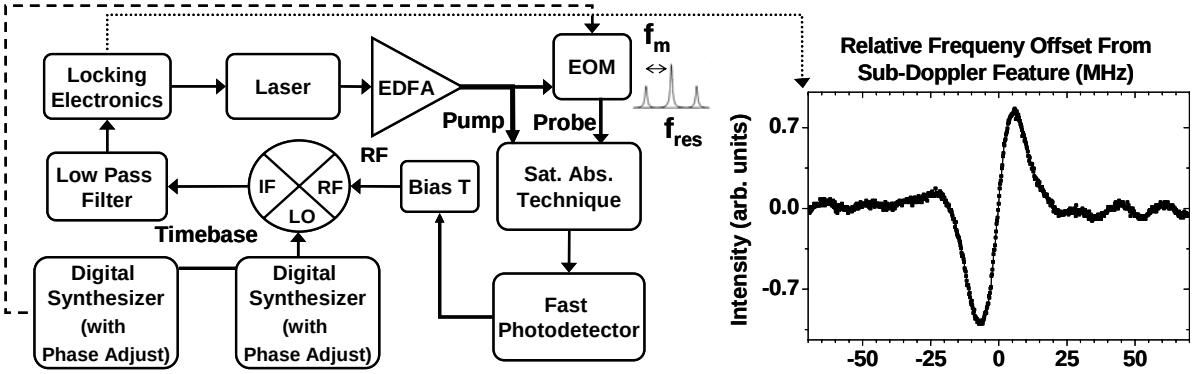

Figure 3. FM spectroscopy setup with spectra of the sub-Doppler derivative. Spectra taken at the following parameters: pressure = 175 mT, pump power (exiting fiber) = 150 mW, f_m = 20 MHz, and S/N = 9.5 dB.

Thanks to Kurt Vogel for helpful discussions of the FM spectroscopy setup, and to NSF and AFOSR for funding.

4. References

[1] S. Ghosh, J. E. Sharping, D. G. Ouzounov, and A. L. Gaeta, "Resonant optical interactions with molecules confined in photonic band-gap fibers," Phys. Rev. Lett. **94**, 093902 (2005).

[2] R. Thapa, K. Knabe, M. Faheem, A. Naweed, O. L. Weaver, and K. L. Corwin, "Saturated absorption spectroscopy of acetylene gas inside large-core photonic bandgap fiber," Opt. Lett. 31, 2489-2491 (2006).

[3] J. Hald, J. C. Petersen, and J. Henningsen, "Saturated Optical Absorption by Slow Molecules in Hollow-Core Photonic Band-Gap Fibers," Phys. Rev. Lett. 98, 213902 (2007).

[4] F. Couny, F. Benabid, P. J. Roberts, P. S. Light, and M. G. Raymer, "Generation and Photonic Guidance of Multi-Octave Optical-Frequency Combs," Science 318, 1118-1121 (2007); F. Couny, F. Benabid, and P. S. Light, "Large-pitch kagome-structured hollow-core photonic crystal fiber," Opt. Lett. 31, 3574-3576 (2006).

[5] P. S. Light, F. Benabid, F. Couny, M. Maric and A. N. Luiten, "Electromagnetically induced transparency in Rb-filled coated hollow-core photonic crystal fiber," Opt. Lett. 32, 1323-1325 (2007).

[6] R. Drever, J. Hall, F. Kowalski, J. Hough, M. Ford, A. Munley, and H. Ward, "Laser Phase and Frequency Stabilization Using an Optical Resonator," Appl. Phys. B 31, 97-105 (1983).

Significant Carrier Envelope Offset Frequency Linewidth Narrowing in a Prism-based Cr:forsterite Frequency Comb

Karl A. Tillman, Rajesh Thapa, Brian R. Washburn and Kristan L. Corwin
Department of Physics, Kansas State University, Manhattan, KS 66506, U.S.A
tillman@phys.ksu.edu

Abstract: We report a dramatic reduction in the linewidth of the carrier envelope offset frequency of a frequency comb generated by a femtosecond prism-based Cr:forsterite laser due to changes in the wavelength-dependent intracavity loss.

OCIS codes: 120.3930 (Metrological instrumentation), 140.3580 (Lasers, solid state), 320.7090 (Ultrafast lasers)

1. Introduction

Optical frequency combs are a very precise way to measure optical frequencies with respect to RF or optical references. These frequency combs have two free parameters: the laser repetition rate (f_r) and the carrier envelope offset frequency (f_0). Often, f_0 is detected using a "self-referencing" technique [1] and the width of this signal reflects a measure of that stability. Although the most stable frequency combs have been obtained with Ti:sapphire lasers, optical wavelengths in the near infrared are more conveniently measured using near IR laser based combs. Fiber lasers have reached stabilities approaching that of Ti:sapphire, but are more limited in their maximum repetition rate. Cr:forsterite is the only near-IR solid-state laser to be stabilized using the "self referencing" technique, but the resulting f_0 beat was unexpectedly wide: 6 MHz as measured in Kim *et al's* chirped mirror based system [2] and 1.5 MHz in our prism-based system [3]. Both these lasers were pumped with a multi-mode Yb:fiber laser, thought to contribute significantly to the f_0 linewidth. We have recently narrowed the f_0 linewidth of our frequency comb by at least two orders of magnitude simply by inserting a knife edge into the laser cavity after the prisms for the purpose of wavelength-tuning the output.

Many studies have been made in Ti:sapphire [4,5] and Er:fiber lasers [6] to understand the dependence of f_0 on pump power (df_0/dP). Indeed the pump power is often used to servo-control the f_0 frequency. Prism-based lasers are known to exhibit both larger and smaller df_0/dP depending on slight changes to intracavity dispersion [4]. The f_0 linewidth (Δf_0) depends on pump power noise [6] and the frequency response rate of the laser [5]. If laser amplitude spectral noise density, $S_\nu(f)$, is white in frequency with units of dBc / Hz, then the key parameters that control Δf_0 are the frequency response of df_0/dP (as set by the gain medium and the laser cavity [6]) and frequency response roll-off of the gain medium [7], which for Ti:sapphire is: f_c = 700 kHz [5]. If df_0/dP changed significantly with the insertion of the knife edge, that could explain the narrowing of Δf_0 .

2. f_0 narrowing and dynamics

Figure 1a shows the laser configuration, with a 10 mm long Brewster-cut crystal of Cr:f, cooled to -5°C and pumped at 1075 nm by 8 W of power from a Yb:fiber laser (IPG Photonics). The pump laser is first passed through an AOM before entering the laser cavity, which is used to control and stabilize f_0. The laser output has a power of ~ 275 mW at a repetition rate of ~ 117 MHz, centered near 1275 nm, and the intracavity prism pair allows the spectral bandwidth to be continuously varied from ~ 35-55 nm.

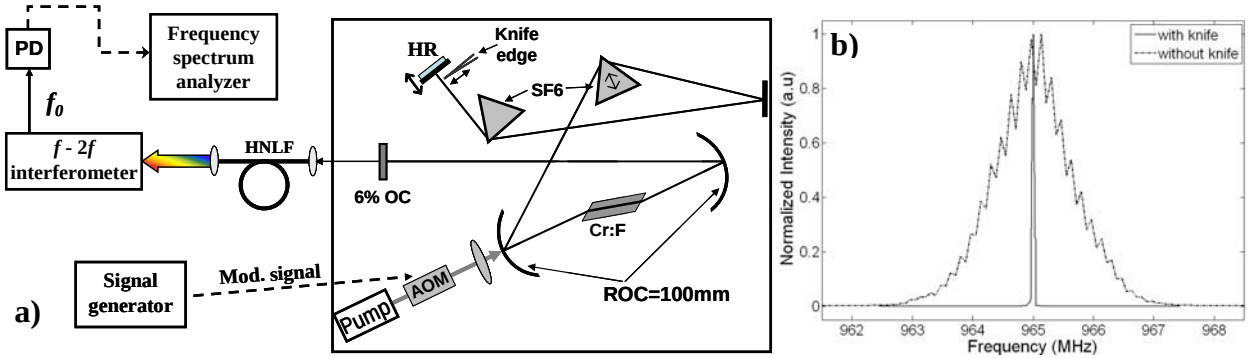

Fig.1: a) Cr:f laser cavity and f_0 detection configuration showing the knife edge, with HR = high reflecting endmirror, OC = output coupler, PD = photodetector. **b)** f_0 linewidth plots with the knife edge inserted (solid) and without the knife (dotted).

This output is then coupled into 10 m of highly-nonlinear fiber (HNLF) to broaden the optical spectrum to span an octave (in our case $\Delta\lambda \rightarrow$ 1.0-2.2 μm), which is then directed into an *f*-to-2*f* interferometer and f_0 is detected after the interferometer using a fast InGaAs photodiode (125 MHz). The knife edge is inserted from the longer wavelength region of the Fourier plane of the prism pair continuously tuning the power spectrum to shorter wavelength, by as much as 20 nm (see Fig.2.b inset). To measure Δf_0 it was first stabilized to some extent using a slow-speed (< 1 kHz) feedback loop to the prism insertion. An RF spectrum analyzer was used to make Δf_0 measurements with and without the knife edge using resolution bandwidths (RBW) of 1 MHz and 30 kHz respectively to measure the normal and narrow profiles. Figure 1b shows the data from these measurements with the knife edge insert (dotted) and without (solid). Without any power modulation Δf_0 for the normal and narrow profiles were ~ 1.5 MHz and < 30 kHz. The response of the slow-servo control of the prism limited our ability to make more precise measurements of the narrow profile. However it did give it an upper limit of Δf_0 = 30 kHz. Previous measurements have shown it to be closer to 10 kHz but this also requires fast servo control of the AOM.

One likely explanation for the reduction in f_0 linewidth with knife edge insertion is that the laser response to power fluctuations has changed considerably, either in amplitude or in frequency response. To test this idea, we again servo-controlled f_0 using the prism insertion and then measured df_0/dP by modulating the pump power with an AOM (whose frequency response was measured to be > 1.3 MHz) with an amplitude of about 4.5% or 350 mW peak-to-peak of the 8 W at frequencies between 250 kHz and 2 MHz. The resulting width of f_0 was measured, and the difference in width from the unmodulated state can then be attributed to the change in pump power. Figure 2a shows the result for both cases, with (dotted line) and without (solid line) the knife edge. The frequency cut-off is about 500 kHz in both cases, but the lack of an abrupt edge in the plot for the absent knife edge must be further explored. The ratio of amplitudes is about a factor 10 but the frequency response cut-off (f_c) is similar in both cases, with a roll-off at around 500 kHz. This increase can be related to df_0/dP by dividing the change in linewidth with and without modulation by the change in pump power, and is not large enough to fully explain the narrowing.

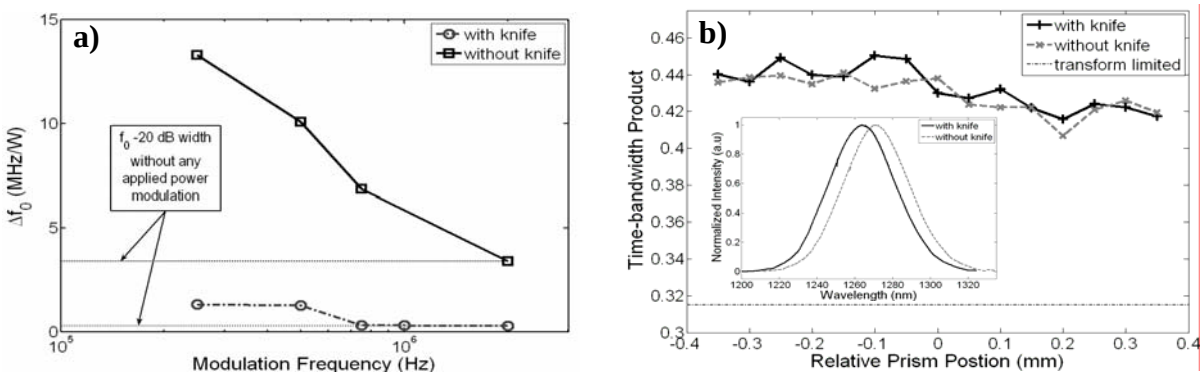

Fig.2: a) frequency response of f_0 width to fast power modulation with (dotted) and without (solid) the knife edge. **b)** Time-bandwidth product for our Cr:f laser with (thick dotted) and without (thick solid) the knife edge inserted compared to the transform limited case (narrow dotted), inset shows the difference in the power spectra with (solid) and without (dotted) the knife edge inserted.

3. Summary

To summarize we report on the dramatic reduction in linewidth of a Cr:f frequency comb simply by tuning the central wavelength of the laser output. The exact cause of the narrowing is not yet fully understood. Further investigations are currently underway to explain the cause of the narrowing and to stabilize the frequency comb with the narrow linewidth to enable us to make an absolute linewidth measurement. The results of these studies will be presented in detail and potential causes for the linewidth reduction will be discussed.

We would like to thank Jeff Nicholson and Man Yan for providing the HNLF, Scott Diddams and Nate Newbury for helpful discussions, and AFOSR and NSF for funding.

[1] D. J. Jones *et al*, 'Carrier envelop phase control of femtosecond modelocked lasers and direct optical frequency synthesis', Science, **288**, p. 635, **2000**

[2] K. Kim *et al*, 'Stabilized frequency comb with a self-referenced femtosecond Cr:forsterite laser', Opt. Lett., **30**, p. 932, **2005**

[3] R. Thapa *et al,* 'Phase-stabilized prism-based Cr:forsterite laser frequency comb for absolute frequency measurements', in Conference on Lasers and Electro-Optics (Optical Society of America, Baltimore, 2006), p. CMKK7

[4] K. W. Holman *et al*, 'Intensity-related dynamics of femtosecond frequency comb', Opt. Lett., **28**, p. 851, **2003**

[5] R. P. Scott *et al*, 'Amplitude and phase noise sensitivity of modelocked Ti:sapphire lasers in terms of a complex noise transfer function', Opt. Exp., **15**, p. 9090, **2007**

[6] B. R. Washburn *et al*, 'Response dynamics of the frequency comb output from a femtosecond fiber laser', Opt. Exp., **13**, p. 10622, **2005**

[7] J. J. McFerran *et al*, 'Suppression of pump-induced frequency noise in fiber-laser frequency combs leading to sub-radian f(ceo) phase excursions', Appl. Phys. B, **86**, p. 219, 2007

Carrier-envelope offset frequency dynamics in a self-referenced prism-based Cr:forsterite frequency comb

Karl A. Tillman, Rajesh Thapa, Brian R. Washburn and Kristan L. Corwin
Department of Physics, Kansas State University, Manhattan, KS 66506, U.S.A

Abstract: **Carrier-envelope offset frequency (f_0) dynamics of a prism-based modelocked Cr:forsterite laser are investigated in the context of a self-referenced frequency comb. Ultimately, this comb will be used in developing acetylene-filled fibers for portable frequency references.**

INTRODUCTION

Considerable scientific interest is currently focused on the development of stabilized frequency combs due to the level of precision and stability they offer to applications such as optical frequency metrology [1], pulse synthesis [2] and high harmonic generation [3]. In these applications the primary concern is to control the carrier-envelope offset frequency (f_0) as this is vital in understanding the nonlinear interactions when using few-cycle femtosecond pulses. Significant progress has been made in the development of self-referenced frequency combs based on solid state lasers such as Ti:sapphire which can offer a frequency stability of the order of sub-hertz with very narrow frequency linewidth. Interest from the telecommunications industry has also helped fuel the development of all fiber based comb systems [4] where there is a need for robust and compact devices capable of easy integration with current technology. Fiber lasers have improved dramatically over recent years [4] and now have narrow linewidths similar to Ti:sapp but lower typical repetition rates. Cr:forsterite lasers have the high repetition rates of other solid state lasers in the near IR, and are therefore of great interest. Kim *et al*. at NIST have previously self-referenced a Cr:f laser based on chirped mirrors [5]. We have phase-stabilized a prism-based Cr:f frequency comb that offers the advantage of greater tuneability of the intracavity dispersion and have observed a narrower f_0 than was measured by the group at NIST [6]. However, the ability to control the parameters of the frequency comb depends on many other parameters, which we are exploring here in order to improve the stability of our comb. We will then use the comb to characterize portable fiber-based frequency reference in the near IR[1] [7].

Any frequency comb has two degrees of freedom that must be controlled in order to generate a fully characterized and phase-stabilized output. These are the repetition frequency (f_{rep}) and the carrier-envelop offset frequency (f_0) and are determined by the group (l/v_g) and phase (l/v_p) delay (where l is the cavity length) of the laser pulses which depend on the total intracavity dispersion of the lasers. Simple servo control of the laser cavity length enables very fine control of f_{rep}; however because the dependence of f_0 on v_g and v_p is more complex, it is significantly harder to control than f_{rep}. A common approach, utilizes the intensity-dependence of the laser gain mediums nonlinear refractive index to change the intracavity dispersion which is achieved by using an acousto-optic modulator (AOM) to modulate the pump power. In the case of prism-based solid state laser systems it has been shown that even for moderate pump power changes there is movement in the intracavity beam [8] changing the optical path around the cavity. This alters the dispersion contributions due to the intracavity prisms which then becomes a function of pump power in addition to the intensity dependence of the nonlinear refractive index of the Cr:f crystal. This means controlling f_0 will be inherently more complex for prism-based systems than for the prismless systems. With this in mind we present preliminary studies of the intensity related dynamics of f_0 for a prism based self-referenced modelocked Cr:f system.

EXPERIMENT

The laser used in this study is based on a folded bow-tie cavity configuration that uses a 10 mm long Brewster angled Cr:f crystal pumped at 1070 nm by a 10 W Yb:fiber laser (IPG Photonics) which is first passed through an AOM. The Cr:f crystal is cooled to -5°C and produces an output centered at 1250 nm with an average power of ~230 mW for pulse durations of ~35 fs at a repetition rate of ~116 MHz. The output is then coupled into ~10 m of highly nonlinear fiber (HNLF) to generate a supercontinuum (SC) output that covers a wavelength range in excess of an optical octave (actual coverage is greater than 1.0-2.2 μm). The output from the HNLF is then directed into an f-to-2f interferometer commonly used in the self-referencing technique. The 2f arm of the interferometer contained a 10 mm long crystal of periodically poled lithium niobate (with a grating period of 30.0 μm) to generate a second harmonic (SHG) of the SC signal at 1030 nm. The SHG signal when mixed with a narrowband filtered section of the SC signal from the f arm of the interferometer (also at 1030 nm) allows the f_0 signal to be detected directly. Both f_{rep} and f_0 were detected simultaneously using a pair of 125 MHz InGaAs photodetectors connected to two independent frequency counters. The modulation in pump power was controlled by an AOM driven by a variable-amplitude, square-wave TTL output from a signal generator. This was synchronized to a frequency modulating (FM) output from the same signal generator which was connected to a third frequency counter. f_{rep}, f_0 and FM were counted

[1] Funding for this project comes from AFOSR under grant no. FA9950-05-1-0304 and from the National Science Foundation under grant No. ECCS-0449295

simultaneously to detect any periodic changes in f_{rep} and f_0 caused by the power modulation. The data were then analyzed to retrieve average Δf_0 values for given prism positions. Measurements were repeated using a range of different prism insertions while the pump power was continually modulated by ~250 mW around 8.9 W at a rate of 5 Hz. The change in power corresponds to an intensity change of ~3.5x10^9 W/m^2 using an estimated pump beam radius of 20 µm.

Figure 1 shows schematically the setup used in the experiment while Fig.2 shows preliminary results of the changes in f_0 for a given pump power change ($\Delta f_0/\Delta P$) across a range of different prism insertion. Figure 2 shows a clear dependency of $\Delta f_0/\Delta P$ on the total intracavity dispersion which will enable the Δf_0 response with pump power to be maximized allowing our servo control of f_0 to become more effective. This investigation along with other studies which are currently underway are necessary to understand the intensity dependant dynamics of f_0 in Cr:f. Using this and other data we hope to develop a theoretical model of the f_0 dynamics similar to that developed for the Ti:sapp laser [9].

Prior to carrying out these studies it was extremely difficult to frequency-lock the f_0 signal due to the presence of large fluctuations (10's of MHz). The magnitude of the pump power changes needed to compensate for these f_0 fluctuations were frequently sufficient to lose modelocked operation of the Cr:f laser. This limited our ability to lock f_0 and use heterodyne detection with a CW laser source in future work to develop portable frequency references. In summary these studies will allow us to develop a better understanding of the more influential aspects of f_0 jitter in prism-based self-referenced Cr:f frequency combs. In addition, these studies have enabled us to develop a method for locking f_0 over extended time periods using a combination of both intracavity prism modulation and pump power modulation.

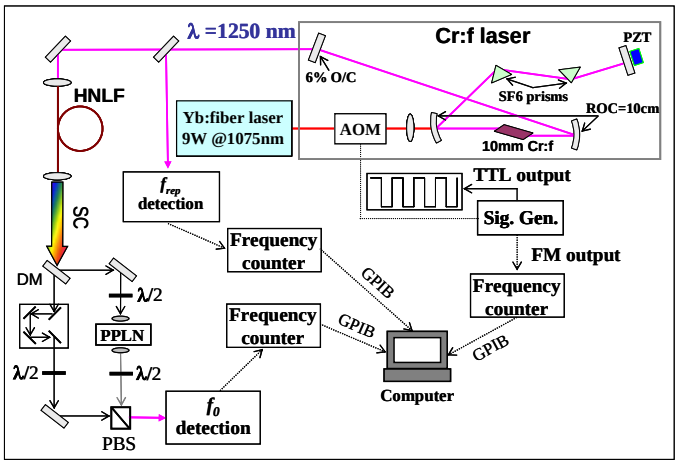

Fig. 1: Experimental configuration used to make $\Delta f_0/\Delta P$ measurements as a function of relative prism insertion. (DM=dichroic mirror, λ/2=half-wave plate, PBS= polarization beam splitter, O/C=output coupler, ROC=radius of curvature, Sig. Gen.=signal generator, all other abbreviations are given in the main text)

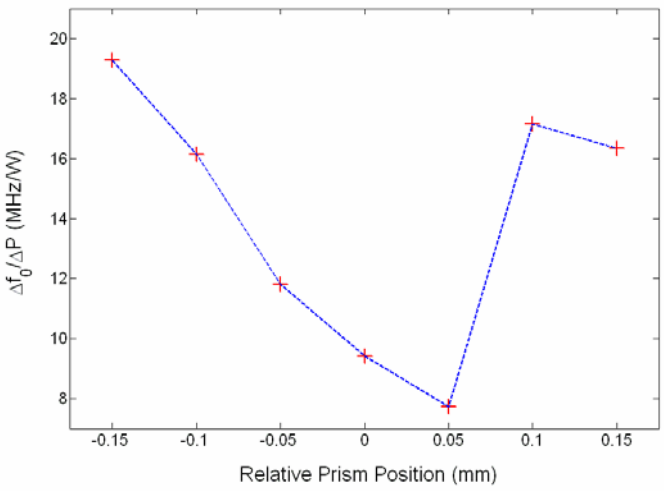

Fig. 2: Preliminary results showing a dependence of the $\Delta f_0/\Delta P$ signal with the relative prism insertion. A minimum in the Δf_0 response of is visible corresponding to a maximum required ΔP needed to maintain a fixed Δf_0.

ACKNOWLEDGMENT

We would like to thank N. Newbury, S. Diddams and K. Read for many helpful discussions and J. Nicholson and M. Yan for supplying the HNLF fiber.

REFERENCES

1. T. R. Schibli, *et al.*, "Frequency metrology with a turnkey all-fiber system". *Opt. Lett.*, 2004. **29**(21): pp. 2467-2469.
2. R. K. Shelton, *et al.*, "Phase-coherent optical pulse synthesis from separate femtosecond lasers". *Science*, 2001. **293**(5533): pp. 1286-1289.
3. A. de Bohan, P. Antoine, D. B. Milosevic,and B. Piraux,, "Phase-dependent harmonic emission with ultrashort laser pulses". *Phys. Rev. Lett.*, 1998. **81**(9): pp. 1837-1840.
4. B. R. Washburn, W. C. Swann, and N. R. Newbury, "Response dynamics of the frequency comb output from a femtosecond fiber laser". *Opt. Exp.*, 2005. **13**(26): pp. 10622-10633.
5. K. Kim, *et al.*, "Stabilized frequency comb with a self-referenced femtosecond Cr : forsterite laser". *Opt. Lett.*, 2005. **30**(8): pp. 932-934.
6. R. Thapa, *et al.*, "Phase-stabilized prism-based Cr:forsterite laser frequency comb for absolute frequency measurements". OSA *CLEO/QELS conference*, 6-11th May 2007. Baltimore, MA, *Conf. Proc.* CMKK7.
7. R. Thapa, *et al.*, "Saturated absorption spectroscopy of acetylene gas inside large-core photonic bandgap fiber". *Opt. Lett.*, 2006. **31**(16): pp. 2489-2491.
8. F. W. Helbing, *et al.*, "Carrier-envelope offset dynamics of mode-locked lasers". *Opt. Lett.*, 2002. **27**(3): pp. 194-196.
9. K. W. Holman, R. J. Jones., A. Marian, S. T. Cundiff, and J. Ye, "Intensity-related dynamics of femtosecond frequency combs". *Opt. Lett.*, 2003. **28**(10): pp. 851-853.

Phase-stabilized Prism-based Cr:forsterite Laser Frequency Comb for Absolute Frequency Measurements

R. Thapa, K. A Tillman, A. Naweed, A. Jones, B. R. Washburn and K. L. Corwin
Kansas State University, Manhattan, KS
rthapa@phys.ksu.edu

J. W. Nicholson and M. F. Yan
OFS Laboratories,19 Schoolhouse Rd., Somerset NJ 08873

Abstract: A prism-based Cr:forsterite frequency comb is stabilized, with a repetition rate of 116 MHz. The flexibility of the prism-based system aids in achieving the carrier-envelope-offset frequency (f_0) beat note width of ~1.5 MHz.

OCIS codes: 120.3940, 320.7090

Optical frequency metrology is a fast growing research field constantly looking for alternative reference sources for a wide range of applications; Cr:forsterite is an appealing gain medium in the near infrared. The output is compatible with telecommunications wavelengths and its gain bandwidth makes it a good alternative to Ti:Sapphire systems for longer wavelength configurations. Previous work using Cr:forsterite by groups at NIST have successfully demonstrated a self-referenced frequency comb, actively stabilized, using a chirped mirror laser design with ~420 MHz repetition rate [1,2]. The laser exhibited excellent long-term stability when compared with Ti:sapphire, but exhibited unusually broad f_0 beat notes with widths of up to 6.7 MHz, attributed to noise during the supercontinuum generation process seeded by the pump laser noise.

Here we report a similar system, with dramatically narrower f_0 beat note widths in spite of employing the same pump laser. The reduced f_0 beat may be due to higher pulse energies, or the added control allowed by the prism. Subtle adjustments in the laser prisms and curved mirror dramatically effect the f_0 beat width and strength. We have developed the first prism-based stabilized Cr:forsterite comb, and intend to reference the comb to a GPS – disciplined rubidium clock, and use the resulting comb to perform absolute frequency measurements of the acetylene $\nu_1+\nu_3$ band absorption lines inside photonic bandgap fiber cells [3].

The laser design is shown below in Fig. 1 a. The pump laser is a cw Yb glass laser with a center wavelength at 1075 nm and with 10 W maximum output. The AOM in the pump beam deflects a variable amount of power in order to achieve f_0 stabilization. The 15 mm long Cr:forsterite crystal has the same bulk properties as that measured in Ref. [4] (doping of 0.2% by weight, absorption coefficient of 1.1cm^{-1} at 1075nm), and a length of 15 mm. Dispersion compensation is achieved in the cavity with an SF6 prism pair, Brewster cut and spaced ~30 cm apart. The laser has an output coupler (E) of 6%, and a PZT-mounted mirror (I) after the second prism for stabilization of the repetition rate. The cavity arms make an angle of ~30^o to compensate astigmatism. For a 1075 nm pump power of 7 W - 9 W, the laser emits ~220 mW, and autocorrelation reveals ~30 fs pulse duration FWHM. To spectrally broaden the laser output, ~200 mW are directed into a dispersion-shifted highly nonlinear fiber (HNLF) with dispersion D = 1.19 ps/(nm km) at 1550 nm. A power of 130 mW emerges from the HNLF fiber, spanning over an octave in bandwidth. The laser and supercontinuum spectra are shown in Fig. 2b, but the supercontinuum spectrum is truncated due to the frequency range of the OSA used to measure the spectrum. Other measurements reveal a large peak in the spectrum at 2040 nm, which is frequency-doubled in a periodically poled lithium niobate (PPLN) crystal and beat against the high-frequency end of the octave to reveal the f_0 beat signal, as is standard in self-referenced combs. The resulting f_0 beat is detected in a New Focus 125 MHz near-IR detector, and sent to an RF spectrum analyzer as well as a loop filter. The rf electronics that act on the f_0 beat are shown in Fig. 1. The repetition rate is detected on a similar detector. The rf electronics filter the f_0 and the repetition frequency (f_r) signals, and feed back to the pump power and cavity length (mirror I), respectively.

Figure 2 a shows the f_0 beat, measured when both f_0 and f_r were locked. That beatnote displays a clear sign of being phase-locked, notably a narrow peak on top of a broad background. However, that narrow peak has width greater than the resolution bandwidth, indicating that the lock is not optimized. Also, the pedestal on which sits the narrow peak is narrower than the beat notes observed by NIST, which we attribute in part to the added control imparted by the prisms. The beatnote is still much wider than those in Ti:sapphire base combs, and the excess noise is most likely due to high-frequency noise on the pump laser. Indeed, by dividing the frequency f_0 by 256 instead of

16, we found that the servo error signal had a clear noise component at about 1.5 MHz, which is difficult to remove with a servo circuit.

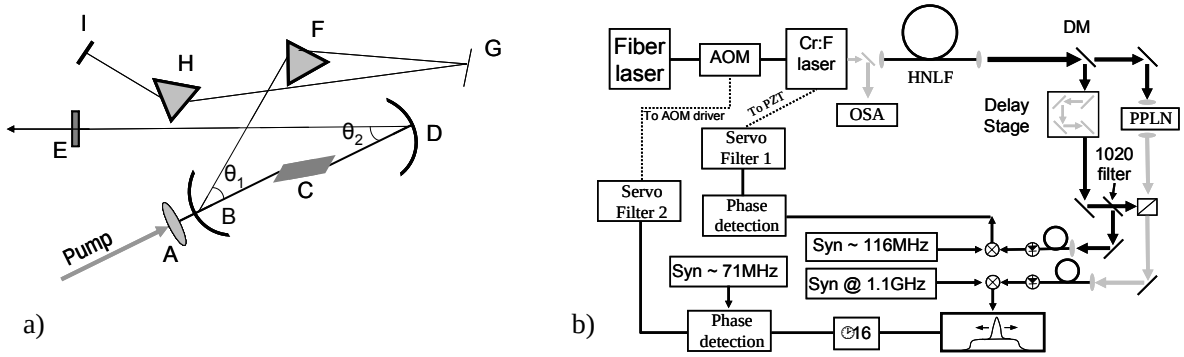

Fig. 1. a) Laser cavity configuration. b) Servo control schematic used to lock f_r and f_0.

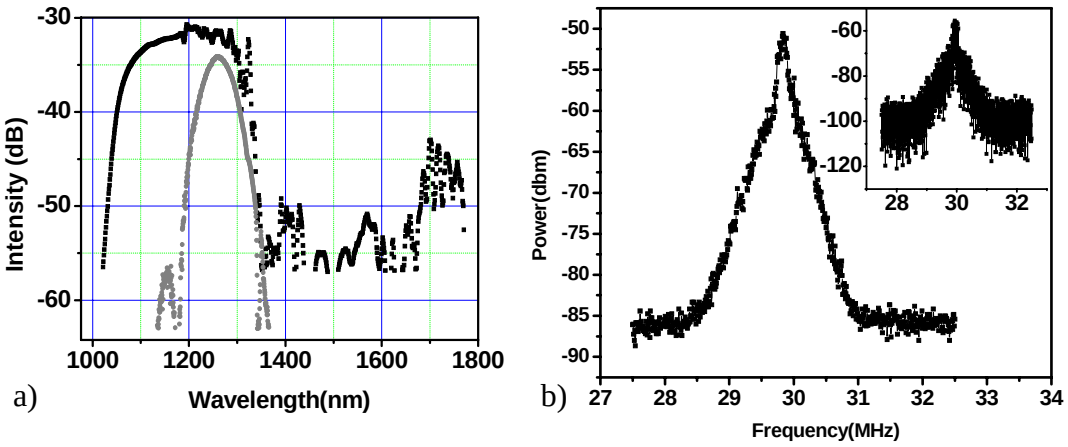

Fig. 2. a) Laser spectrum (grey) and supercontinuum spectrum (black). The spectrum does not show the significant optical power beyond 1.7 μm, where the OSA is no longer sensitive. b) f0 beat measured on rf spectrum analyzer with RBW of 30 kHz and a reduced video BW. Inset shows same signal, with Resolution BW = Video BW = 30 kHz. (inset). The narrow feature has a width of ~ 200 kHz, and the larger feature has a width of ~1.5 MHz.

Next, we plan to reference the synthesizers to a GPS-stabilized Rb clock. Then we plan to characterize the long-term stability of the acetylene-filled fiber-based references that we are currently developing [3]. Ultimately, such references may prove advantageous as a high-short-term stability reference for a portable optical frequency comb.

Acknowledgements: We thank S. Diddams, K. Read, and H. Kapteyn for their efforts in designing the laser, and N. Newbury for helpful discussions. This work is funded by AFOSR and NSF.

References:

[1] K. Kim, S.A. Diddams, P.S. Westbrook, J.W. Nicholson, and K.S. Feder, "Improved stabilization of a 1.3 mm femtosecond optical frequency comb by use of a spectrally tailored continuum from a nonlinear fiber grating," Opt. Lett., **31**, 277 (2006).

[2] K. Kim, B. R. Washburn, G. Wilbers, C. W. Oates, L. Hollberg, N. R. Newbury, S. A. Diddams, J. W. Nicholson, and M. F. Yan, "Stabilized frequency comb with a self-referenced femtosecond Cr:forsterite laser," Opt. Lett., **30**, 932 (2005).

[3] R. Thapa, K. Knabe, M. Faheem, A. Naweed, O. L. Weaver, and K. L. Corwin, "Saturated absorption spectroscopy of acetylene gas inside large-core photonic bandgap fiber," **31**, 2489 (2006).

[4] I. Thomann, L. Hollberg, S. A. Diddams, and R. Equall, "Chromium-doped forsterite: dispersion measurement with white-light interferometry," Appl. Opt., **42**, 1661.

Reflected Pump Technique for Saturated Absorption Spectroscopy Inside Photonic Bandgap Fibers

Kevin Knabe, Rajesh Thapa, Brian R. Washburn, and Kristan L. Corwin
Kansas State University, 116 Cardwell Hall, Manhattan, KS 66506.
corwin@phys.ksu.edu

Abstract: Saturated absorption spectroscopy in acetylene-filled photonic bandgap fibers is investigated. A new simplified technique for saturated absorption spectroscopy is described, where pressure and power parameters have been optimized for use as a frequency reference.

OCIS codes: (300.6460) Spectroscopy, saturation; (060.2310) Fiber optics

Photonic bandgap fibers (PBGF) exhibit low loss and facilitate nonlinear interactions between light and gases or liquids confined in the core. Both electromagnetically induced transparency (EIT) and saturated absorption spectroscopy have been observed in various gases in these fibers [1-4]. Sealed fibers have also been developed as vapor cells [5]. Here we demonstrate a novel method of saturation absorption using only one beam inside hollow photonic bandgap fibers.

Previously, we have reported saturated absorption spectroscopy inside acetylene-filled PBGF [4]. Acetylene-filled PBGF exhibit narrow features when used in saturated absorption spectroscopy, as in Fig. 1a. The width and strength of the saturated absorption feature is dependent on pressure, optical power, and fiber core diameter. These parameters have been optimized for maximum signal strength and minimum width.

1a)

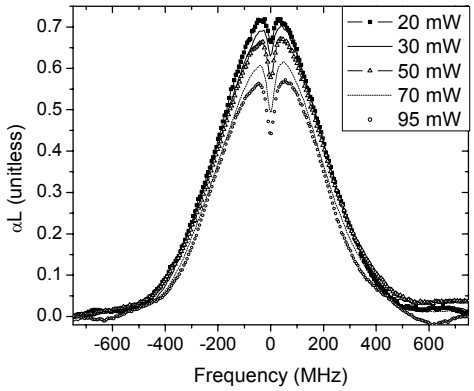

1b)

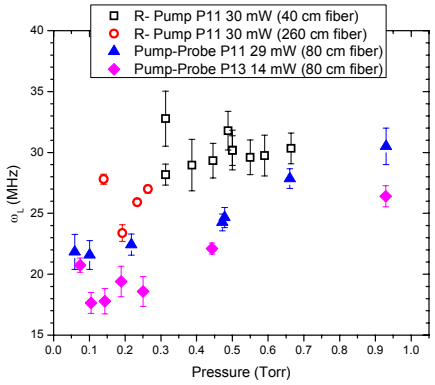

Fig. 1. Absorption spectra and fitting results. a) The above time-averaged spectra were taken of the C_2H_2 $\nu_1+\nu_3$ P(11) vibrational line at an optical wavelength of ~ 1.53 μm at a constant acetylene pressure of 0.50 Torr, for a 40 cm long photonic bandgap fiber, with a 20 μm diameter core. One can see that the overall amplitude of the Doppler-broadened feature decreases as the pump power increase from 20 to 95 mW. b) Sub-Doppler Widths vs. Pressure. These widths are results of the fitting of time averaged saturated absorption spectra of the C_2H_2 $\nu_1+\nu_3$ P(11) and P(13) vibrational lines inside 20 μm PBGF at an optical wavelength of ~ 1.53 μm. The pump power of each measurement was 30 mW except for the P(13) line, which was done at 14 mW.

The transmission through the fiber is measured as a function of laser frequency. The resulting spectra are interpreted using Beer's Law, which describes the transmission of light through matter as $P = P_0 e^{-\alpha_s L}$ where P_0 is the incident power, P is the transmitted power, and L is the length of the fiber. Fig. 1a shows α_s L as a function of laser frequency, for different powers. The signal strength and signal width of the sub-Doppler feature have been measured as functions of both power and pressure inside PBGF diameters of 10 and 20 μm where larger line widths and reduced signal-to noise ratio were observed in the 10 μm fibers, as compared with 20 μm fibers. Interference between the probe beam and undesirable reflections of the pump beam was a significant problem, prompting the insertion of an acousto-optic modulator (AOM) in the probe beam path (Fig. 2b). Half-cells comprised of PBG fibers that are spliced to SMF28 (with only one end attached to a vacuum system) have also been investigated. Spliced fibers also exhibit loss due to reflections at the splice boundary, as well as mode mismatching.

A new technique has been discovered that utilizes the splice in these half-cells. This technique is similar to methods previously explored in glass vapor cells [6] and optical fiber setups using retro reflectors [3], but to our

knowledge has never before been realized by utilizing reflections from the fiber cavity itself. Instead of using a traditional pump and probe beam setup, only a pump beam is present (Fig. 2a and 2b). This new method, called the reflected pump technique, uses about half the optics that the traditional method calls for, and has an added benefit of having much less pump-probe interference than the traditional pump-probe technique does (when the pump-probe technique is used without interference reduction methods such as AOMs or careful polarization management). The reflection at the splice caused by the glass-to-air interface acts as a probe. This probe is less than 10% of the pump beam, which differs from the retro reflecting techniques where the entire pump beam is reflected. Also, in the fiber based retro reflecting setup [6], free-space coupling is required to obtain this reflection, wherein our technique inherently creates the reflection within the fiber.

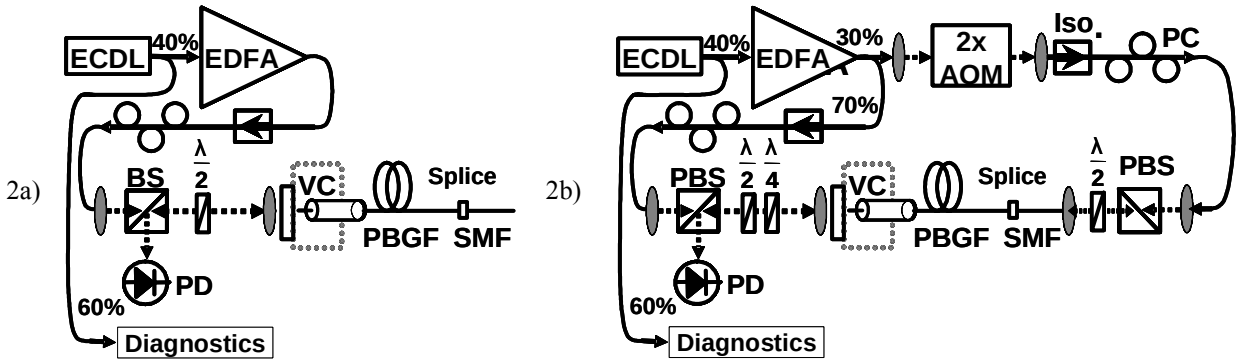

Fig. 2. Reflected Pump setup compared to a typical setup. a) Simplified schematic of this invention, in which the probe beam is created at the splice interface between the PBGF and SMF. b) Schematic of the traditional pump-probe configuration for saturated absorption spectroscopy. The probe beam, after being frequency-shifted by means of a double-passed AOM, is spatially coupled into the SMF end of the spliced half-cell.

Some interesting features arise from this new technique. The most prominent difference is that if one performs both techniques on the same spliced fiber, the amplitude of the absorption profile (α_s L) of the R-Pump technique is twice as large as that of the traditional technique at low powers. This is due to the fact that we are using the pump to create the probe, which therefore has twice the overall path length compared to the path length of the probe in the traditional pump-probe technique. In contrast, however, the width and the depth of the sub-Doppler feature remains approximately unchanged between the two methods (Fig. 1b illustrates the comparison of the widths). The amplitude of the Doppler broadened profile also decreases as pump power increases because the pump saturates the acetylene molecules reducing absorption (Fig. 1a). The probe beam, because it is weak compared to the pump, does not appreciably saturate the sample, maintaining a narrow line.

We gratefully acknowledge helpful discussions with Larry Weaver and funding from AFOSR and NSF.

[1] S. Ghosh, J. E. Sharping, D. G. Ouzounov, and A. L. Gaeta, "Resonant Optical Interactions with Molecules Confined in Photonic Band-Gap Fibers," Phys. Rev. Lett. **94**, 093902 (2005).

[2] P. S. Light, F. Couny, F. Benabid, and P. S. J. Russell, "Electromagnetically-Induced Transparency and Saturable Absorption in All -Fiber Devices Based on Acetylene-Filled Hollow-Core PCF," in *Proceedings of European Conference on Optical Communication 2005 proceedings*, 6, 2005) 59.

[3] J. Henningsen, J. Hald, and J.C. Petersen, "Saturated absorption in acetylene and hydrogen cyanide in hollow-core photonic bandgap fibers," Opt. Exp. **13**, 10475-10482 (2005).

[4] R. Thapa, K. Knabe, M. Faheem, A. Naweed, O. L. Weaver, and K. L. Corwin, "Saturated absorption spectroscopy of acetylene gas inside large-core photonic bandgap fiber," Opt. Lett. **31**, 2489-2491 (2006).

[5] F. Benabid, F. Couny, J. C. Knight, T. A. Birks, and P. S. J. Russell, "Compact, stable and efficient all -fibre gas cells using hollow-core photonic crystal fibres," Nature **434**, 488-491 (2005).

[6] M. Wheel and A. Kumarakrishnan, "Laser-frequency stabilization using a lock-in amplifier," Can. J. Phys. 83: 907–918 (2005).

Comparison of Saturated Absorption Spectra of Acetylene Gas Inside Photonic Bandgap Fibers

K. Knabe, R. Thapa, O. L. Weaver, B. R. Washburn, and K. L. Corwin

Kansas State University, Dept. of Physics, 116 Cardwell Hall, Manhattan, KS 66506
email: corwin@phys.ksu.edu, phone: 785-532-2263, fax: 785-532-6606

Abstract: Saturated absorption spectroscopy is performed inside hollow photonic bandgap fibers, with both 10 μm and 20 μm core diameters. Line width and signal quality depend on the fiber core diameter, as well as pressure and optical power. These parameters are optimized toward the creation of an optical reference. The effect of splicing the fiber to a single-mode fiber is also investigated.

The development of optical frequency standards in the near-infrared spectral region has been motivated in part by the optical telecommunications industry. Acetylene gas offers a series of well-spaced spectral features in the 1.5 μm region, spanning the C band. By pressure-broadening these features to about 1 GHz in width, the National Institute of Standards and Technology (NIST) has created portable standards of moderate uncertainties, between 13 MHz and 130 MHz, that can be built into commercial devices [1, 2]. Meanwhile, sub-Doppler spectroscopy of molecular gases provides high-accuracy infrared optical frequency references. Typically the weak molecular overtone transitions employed at these wavelengths require high powers for saturation, and therefore to date all high-accuracy references have been based on power build-up cavities [3, 4] , which provide power amplification and long effective interaction lengths but are not readily portable. A series of measurements of lines in the $\nu_1 + \nu_3$ band [4-6] led the Comitté International des Poids et Mesures (CIPM) to adopt a value of the P(16) line in $^{13}C_2H_2$ with an uncertainty of 100 kHz [7]. With the advent of frequency comb technology, groups at the National Institute of Advanced Industrial Science and Technology (AIST) in Japan [8, 9], National Physical Laboratory (NPL) in the UK [10], and the National Research Council (NRC) in Canada [11, 12] have measured these lines with greatly increased precision. The CIPM recently reduced the uncertainty of the P(16) transition to 10 kHz, and most recently, 61 lines in the band have been realized with a width of 600 kHz and measured to an uncertainty of 1.4 kHz [13]. However, there are many advantages to performing saturation spectroscopy independent of a power build-up cavity, as described in Ref. [14], where signals with widths ~1 MHz have been observed inside a 1 m long glass cell.

While the science of frequency metrology has been transformed, optical fiber technology has simultaneously been revolutionized by the advent of hollow, low-loss photonic bandgap (PBG) fibers. These optical waveguides allows light to be confined at high intensities in a hollow air or gas-filled region with very low loss [15]. These fibers are vastly superior to capillary fibers for small core diameters [16], and have therefore been used in many recent demonstrations of nonlinear light-gas interactions. Examples include gas sensors [17], Raman scattering in hydrogen-filled fiber as a tunable light source [18], and electromagnetically induced transparency (EIT) in PBG fibers filled with acetylene and rubidium [19-21]. Lasers have been locked to the side of Doppler-broadened transitions in sealed acetylene-filled fibers, toward the development of portable frequency references [22]. Finally, saturated absorption has been observed inside photonic bandgap fibers. Initial observations indicated large background noise arising from interference and mode beating [23, 24], even in an all-fiber configuration [25]. A more complete discussion of these issues appears in Ref. [26].

For PBG fiber cells to be employed as frequency references, the saturated absorption spectrum must be optimized in magnitude and minimized in width. Also, modulation of the transmitted light due to spurious interference or mode beating must be suppressed. In the effort to develop optical frequency references using acetylene filled PBG fiber cells, we have examined the dependence of signal size and width on gas pressure and fiber diameter, among other factors. Furthermore, when the PBG fiber is sealed by splicing SMF solid-core fiber to either side, etalon effects and changes in mode coupling may give rise to spurious signals that must be minimized. Thus we characterize saturated absorption inside a PBG fiber, as a function of gas and fiber dimensions. We also investigate the effects of splicing the fiber on the signal quality.

In Fig. 1a, the experimental setup is shown for measurements of acetylene saturated absorption spectra in an isolated photonic bandgap fiber. Modifications to the experiment made to accommodate a single splice between a step-index single-mode fiber and a photonic bandgap fiber are shown in Fig. 1b. The details of the splicing technique for splicing hollow PBG fiber to step-index fiber are given in Ref. [27]. A 5 mW beam from an extended cavity diode laser (ECDL) is split, and 10% is amplified by an IPG Photonics® Erbium-doped fiber amplifier (EDFA) to up to 500 mW. The remaining power is sent to diagnostics, which include an acetylene-filled glass cell

(as in Ref. [1]), in order to locate the relevant transitions, and a Michelson interferometer, used to monitor the laser frequency as it is swept across the transition under study. The output from the EDFA is split into pump and probe beams, and the probe passes through an acousto-optic modulator (AOM) in order to shift the frequency between the pump and probe beams, minimizing the interference between the probe and any stray pump light. To compensate for polarization rotation inside the fibers, half-wave and quarter-wave plates are used to cleanly separate the pump and probe beams. Also shown are isolators (Iso.), polarization controllers (PC), polarizing beam splitters (PBS), the vacuum chambers (VC), and a photodetector (PD). In Fig. 1b, the second vacuum chamber is obviated by a fusion splice which seals one end of the PBG fiber. Two different PBG fiber types are investigated, as indicated in Fig. 1c and d, with 10 μm and 20 μm nominal core diameters, respectively.

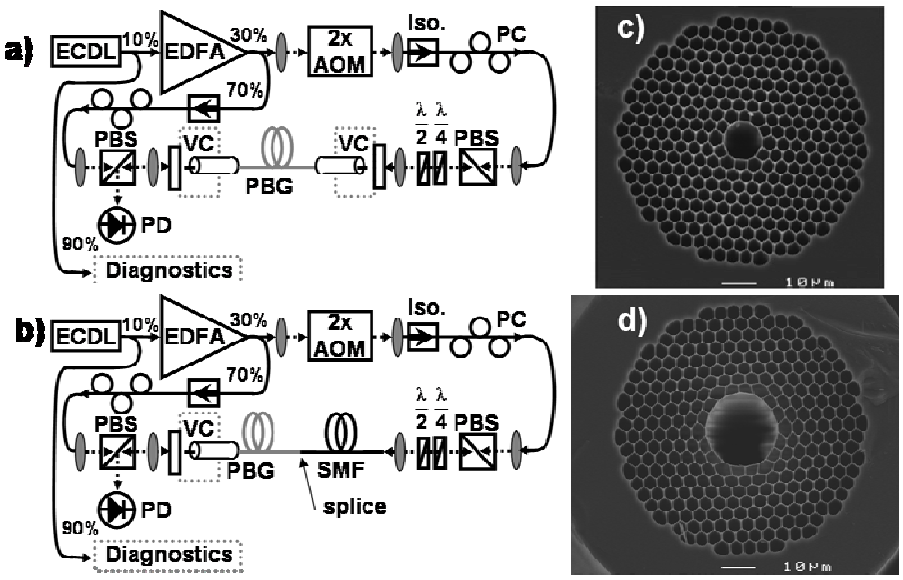

Fig. 1. a) Schematic of the experimental setup, for unspliced fibers. b) Same as a, but with one end of fiber spliced to SMF. c) 10 μm core PBG fiber, made by Crytal Fibre HC-1550-02. d) 20 μm core PBG fiber, made by Crytal Fibre HC19-1550-01. Images of fiber cross-sections provided by Crystal Fibre A/S, www.crystal-fibre.com.

The dependence of the observed signal size inside the 20 μm diameter fiber is shown in Fig. 2a. The central dip in transmitted power is due to the presence of the pump beam, which burns a Bennett hole in the ground-state population of the acetylene molecules. When the probe and the pump are resonant with the same velocity class of molecules, the probe light is less strongly absorbed. A laser may be locked to this feature and used as a frequency reference. Both the strength of the absorption and the width of the saturated absorption feature increase with pressure. Off resonance, the wings are very flat. In contrast, Fig. 2b is taken in a 10 μm fiber, and reveals large interference in the wings, indicative of mode beating. The difference between the two spectra is likely due to a reduced number of surface modes [28] present in the larger-core fiber.

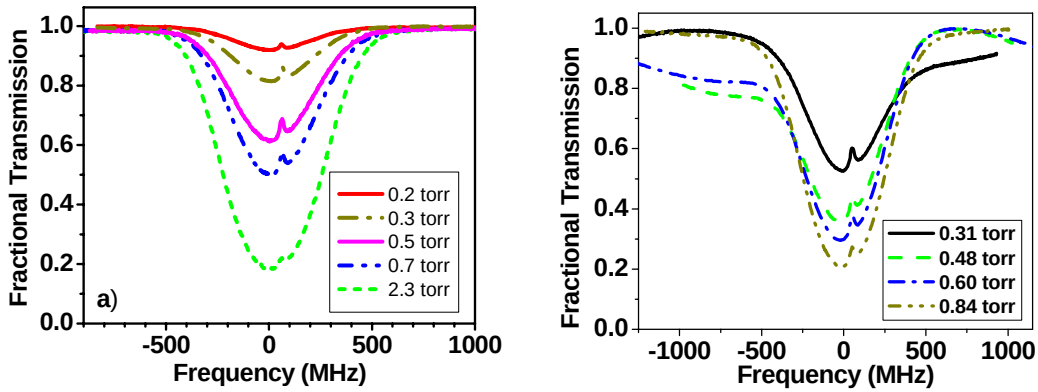

Fig. 2. a) Fractional transmission versus optical frequency detuning at different gas pressures, for the $^{12}C_2H_2$ P (11) transition with a pump power of 29 mW incident on the 0.78 m long fiber. b) Same as a), but in the 10 μm with length 0.90 m long and 30 mW of pump power.

The above spectra are interpreted in terms of Beer's law [29], which describes the transmission of light through a medium as $P = P_0\, e^{-\alpha s(\nu) l}$, where P_0 is the incident power, P is the transmitted power, and l is the length of the medium. From P_0 and P is calculated $l\ \alpha_s(\nu)$, as shown in Fig. 3a. Then $l\ \alpha_s(\nu)$ is fit to an appropriate function, taking into account the Gaussian nature of the Doppler broadened signal and the Lorentzian saturation dip [26]. The full-width-half-maximum w of this Lorentzian feature is plotted as a function of gas pressure in Fig. 3b, for two different pump powers, in the 20 μm fiber with length 0.78 m. Figure 3c shows the frequency discrimination of the saturated absorption feature, which is the signal height in fractional absorption divided by the signal width in MHz. Larger values indicate increased suitability for an optical frequency reference. From Figs. 2 and 3, it is clear that the 20 μm fiber provides cleaner signals and narrower signals than the 10 μm fiber. Thus the 20 μm fiber is more suitable for a frequency reference.

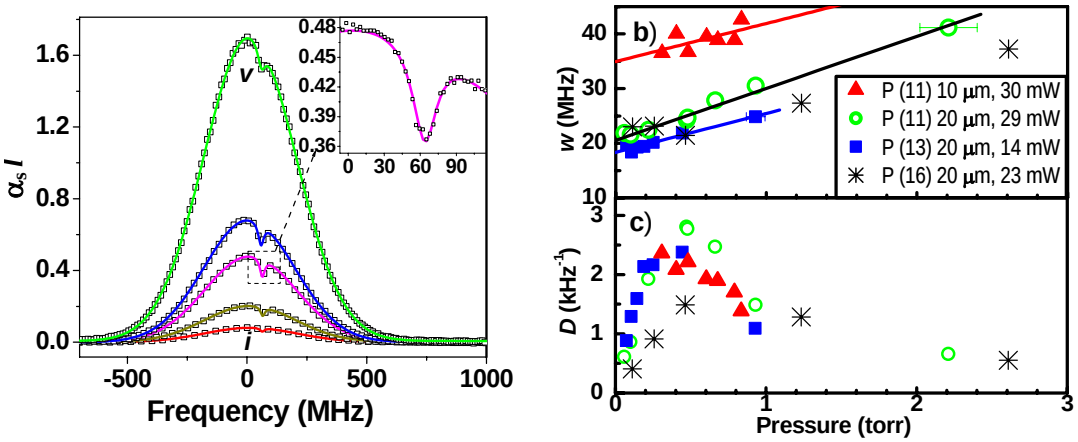

Fig. 3. a) $\alpha_s l$ calculated for the data shown in Fig. 2a, from top to bottom in order of decreasing pressure. Solid lines represent fits to the above equation, using the function described above. b) Width vs. pressure resulting from fits. Circles represent widths of Lorentzian features shown at left. Squares and asterisks represent different transitions interrogated within the same fiber, at the pump powers shown. Triangles represent the widths found in a 10 μm fiber with length 0.90 m. c) Frequency discrimination of the saturation dip, indicating the suitability of the standard for a frequency reference.

In order to employ these PBG fibers as frequency references, they must be sealed by splicing solid-core fiber to each end. Typically this is done with more costly filament heater splicers, but we have demonstrated low-loss splices using a conventional arc splicer [27]. In Fig. 4, spectra taken in spliced fibers are compared to those from unspliced fibers. While the background oscillations in the 10 μm fibers are similar with and without splices, the very flat background offered in the 20 μm fiber is degraded in the presence of the splice. This is most likely due to reflections in the fiber, but may also be due to different coupling into the surface modes of the fiber when using spliced fiber instead of free-space coupling. Further investigation is warranted.

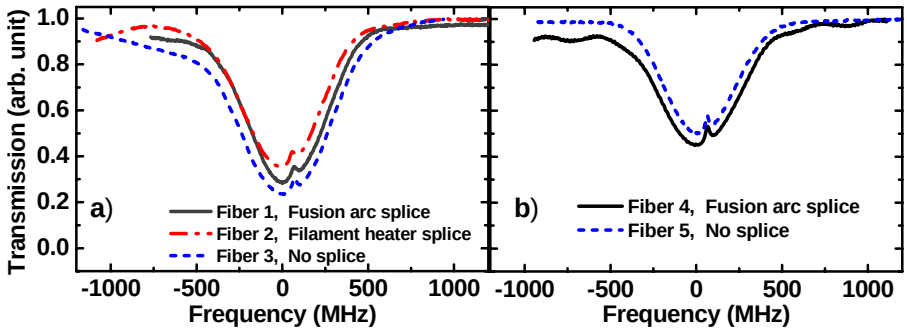

Figure 4. Saturated absorption spectra in a) 10 μm and b) 20 μm diameter PBG fibers. Fiber 1 is 0.78 m long, spliced to SMF using a conventional arc splicer, as described in Ref. [27], and the P(11) spectrum was taken at 29 mW and 0.86 torr. Fiber 2 is 2.0 m long, spliced to SMF by Crystal Fibre A/S using a filament heating splicer, and the spectrum is taken of the weaker P(12) transition at 17 mW and 0.81 torr. Fiber 3 is the unspliced 10 μm fiber of Fig. 2b, of P(11) at 0.69 torr. Fiber 4 is 43.5 cm long, spliced with an arc splicer to SMF, taken of P(11) at 43 mW and 0.8 torr. Fiber 5 is the 20 μm fiber of Fig. 2a, at ~ 0.7 torr.

We gratefully acknowledge funding from AFOSR, and NSF EPSCoR and CAREER. We thank Sarah Gilbert, Dirk Müller, Ahmer Naweed, Bill Swann, and Kurt Vogel for helpful discussions, and Mike Wells and the J. R. Macdonald laboratory staff for technical support.

References

[1] W. C. Swann and S. L. Gilbert, "Pressure-induced shift and broadening of 1510 - 1540-nm acetylene wavelength calibration lines," J. Opt. Soc. Am. B **17**, 1263 - 1270 (2000).

[2] S. L. Gilbert and W. C. Swann, "Acetylene $^{12}C_2H_2$ absorption reference for 1510 nm to 1540 nm Wavelength Calibration -- SRM 2517a," 2001.

[3] M. d. Labachelerie, K. Nakagawa, and M. Ohtsu, "Ultranarrow $^{13}C_2H_2$ saturated-absorption lines at 1.5 μm," Opt. Lett. **19**, 840 - 842 (1994).

[4] K. Nakagawa, M. d. Labachelerie, Y. Awaji, and M. Kourogi, "Accurate optical frequency atlas of the 1.5-μm bands of acetylene," J. Opt. Soc. Am. B **13**, 2718 - 2714 (1996).

[5] A. Onae, T. Ikegami, K. Sugiyama, F. L. Hong, K. Minoshima, H. Matsumoto, K. Nakagawa, M. Yoshida, and S. Harada, "Optical frequency link between an acetylene stabilized laser at 1542 nm and an Rb stabilized laser at 778 nm using a two-color mode-locked fiber laser," Optics Communications **183**, 181-187 (2000), <Go to ISI>://000089153500021.

[6] A. Onae, K. Okumura, K. Sugiyama, F.-L. Hong, H. Matsumoto, K. Nakagawa, R. Felder, and O. Acef, "Optical Frequency Standard at 1.5 μm based on Doppler-free acetylene absorption," in *Proceedings of 6th Sypm on Frequency Standards and Metrology*, P. Gill, (World Scientific, Singapore, 2002) 445.

[7] T. J. Quinn, "Practical realization of the definition of the metre, including recommended radiations of other optical frequency standards (2001)," Metrologia **40**, 103 (2003).

[8] F.-L. Hong, A. Onae, J. Jiang, R. Guo, H. Inaba, K. Minoshima, T. R. Schibli, H. Matsumoto, and K. Nakagawa, "Absolute frequency measurement of an acetylene-stabilized laser at 1542 nm," Opt. Lett. **28**, 2324-2326 (2003).

[9] J. Jiang, A. Onae, H. Matsumoto, and F. L. Hong, "Frequency measurement of acetylene-stabilized lasers using a femtosecond optical comb without carrier-envelope offset frequency control," Opt. Express **13**, 1958-1965 (2005).

[10] C. S. Edwards, H. S. Margolis, G. P. Barwood, S. N. Lea, P. Gill, G. Huang, and W. R. C. Rowley, "Absolute frequency measurement of a 1.5-μm acetylene standard by use of a combined frequency chain and femtosecond comb," Opt. Lett. **29**, 566-568 (2004).

[11] A. Czajkowski, J. E. Bernard, A. A. Madej, and R. S. Windeler, "Absolute frequency measurement of acetylene transitions in the region of 1540 nm," Appl. Phys. B **79**, 45-50 (2004).

[12] A. Czajkowski, A. A. Madej, and P. Dube, "Development and study of a 1.5 μm optical frequency standard referenced to the P(16) saturated absorption line in the (v(1)+v(3)) overtone band of $^{13}C_2H_2$," Optics Communications **234**, 259-268 (2004).

[13] C. S. Edwards, H. S. Margolis, G. P. Barwood, S. N. Lea, P. Gill, and W. R. C. Rowley, "High-accuracy frequency atlas of $^{13}C_2H_2$ in the 1.5 μm region," Appl. Phys. B **80**, 977 (2005).

[14] A. Onae, K. Okumura, Y. Miki, T. Kurosawa, E. Sakuma, J. Yoda, and K. Nakagawa, "Saturation spectroscopy of an acetylene molecule in the 1550 nm region using an erbium doped fiber amplifier," Opt. Comm. **142**, 41 (1997).

[15] R. F. Cregan, B. J. Mangan, J. C. Knight, T. A. Birks, P. S. Russell, P. J. Roberts, and D. C. Allan, "Single-mode photonic band gap guidance of light in air," Science **285**, 1537-1539 (1999), <Go to ISI>://000082359500056.

[16] F. Benabid, J. C. Knight, G. Antonopoulos, and P. S. J. Russell, "Stimulated Raman Scattering in Hydrogen-Filled Hollow-Core Photonic Crystal Fiber," Science **298**, 399 (2002).

[17] T. Ritari, J. Tuominen, H. Ludvigsen, J. C. Petersen, T. Sørensen, T. P. Hansen, and H. R. Simonsen, "Gas sensing using air-guiding photonic bandgap fibers," Opt. Express **12**, 4081 (2004).

[18] F. Benabid, G. Bouwmans, J. C. Knight, P. S. J. Russell, and F. Couny, "Ultrahigh Efficiency Laser Wavelength Conversion in a Gas-Filled Hollow Core Photonic Crystal Fiber by Pure Stimulated Rotational Raman Scattering in Molecular Hydrogen," Phys. Rev. Lett. **93**, 123903-1 (2004).

[19] S. Ghosh, J. E. Sharping, D. G. Ouzounov, and A. L. Gaeta, "Resonant Optical Interactions with Molecules Confined in Photonic Band-Gap Fibers," Phys. Rev. Lett. **94**, 093902 (2005).

[20] F. Benabid, P. S. Light, F. Couny, and P. S. Russell, "Electromagnetically-induced transparency grid in acetylene-filled hollow-core PCF," Opt. Express **13**, 5694-5703 (2005).

[21] S. Ghosh, A. R. Bhagwat, C. K. Renshaw, S. Goh, A. L. Gaeta, and B. J. Kirby, "Nonlinear Optical Interactions with Rubidium Atoms Confined in a Hollow-Core Photonic Crystal Fiber," in *Proceedings of Conference on Lasers and Electro-Optics (CLEO)*, (Optical Society of America, 2006)

[22] F. Benabid, F. Couny, J. C. Knight, T. A. Birks, and P. S. J. Russell, "Compact, stable and efficient all-fibre gas cells using hollow-core photonic crystal fibres," Nature **434**, 488-491 (2005).

[23] M. Faheem, R. Thapa, and K. L. Corwin, "Spectral Hole Burning of Acetylene Gas inside a Photonic Bandgap Optical Fiber," in *Proceedings of Conference on Lasers and Electro-optics (CLEO)*, (Optical Society of America, 2005)

[24] J. Henningsen, J. Hald, and J. C. Petersen, "Saturated absorption in acetylene and hydrogen cyanide in hollow-core photonic bandgap fibers," Optics Express **13**, 10475 (2005).

[25] P. S. Light, F. Couny, F. Benabid, and P. S. J. Russell, "Electromagnetically-Induced Transparency and Saturable Absorption in All-Fiber Devices Based on Acetylene-Filled Hollow-Core PCF," in *Proceedings of European Conference on Optical Communication 2005 proceedings*, 6, 2005) 59.

[26] R. Thapa, K. Knabe, M. Faheem, A. Naweed, O. L. Weaver, and K. L. Corwin, "Saturated absorption spectroscopy of acetylene gas inside large-core photonic bandgap fiber," Opt. Lett. ***(in press)*** (2006).

[27] R. Thapa, K. L. Corwin, and B. R. Washburn, "Splicing Hollow-Core Photonic Bandgap Fiber to Step-Index Fibers Using an Arc Fusion Splicer," in *Proceedings of Conference on Lasers and Electro-Optics (CLEO)*, (Optical Society of America, 2006)

[28] J. A. West, C. M. Smith, N. F. Borrelli, D. C. Allan, and K. W. Koch, "Surface modes in air-core photonic band-gap fibers," Opt. Express **12**, 1485-1496 (2004).

[29] W. Demtröder, *Laser Spectroscopy*: Springer, 1996.

Saturated Absorption Signals from Acetylene Gas Inside Photonic Bandgap Fiber

R. Thapa, K. Knabe, A. Naweed, M. Faheem, O. L. Weaver, and K. L. Corwin

Kansas State University, Dept. of Physics, 116 Cardwell Hall, Manhattan, KS 66506
email: corwin@phys.ksu.edu, phone: 785-532-2263, fax: 785-532-6606

Abstract: Saturated absorption spectroscopy signals inside a 20 μm diameter acetylene-filled photonic bandgap fiber are optimized for use as optical frequency references. Modeling of the light propagation along the fiber reveals a low saturation intensity.

OCIS codes: (060.2310) Fiber Optics ; (300.6460) Saturation Spectroscopy;

Acetylene is used extensively for frequency standards in the near-infrared [1-4]. Photonic bandgap (PBG) fiber allows light and gas to be confined to a small area over long interaction lengths, facilitating nonlinear interactions such as Raman scattering [5], electromagnetically-induced transparency [6] , and saturated absorption spectroscopy [7]. Here, we demonstrate saturated absorption inside PBG fibers with high signal-to-noise ratio, and measure a low saturation intensity (~35 mW). We also identify the optimum operation parameters for a given fiber length and diameter. In Fig. 1, the transmitted probe power versus frequency reveals saturated absorption features inside PBG fibers at a variety of pressures, for a pump power of 29 mW.

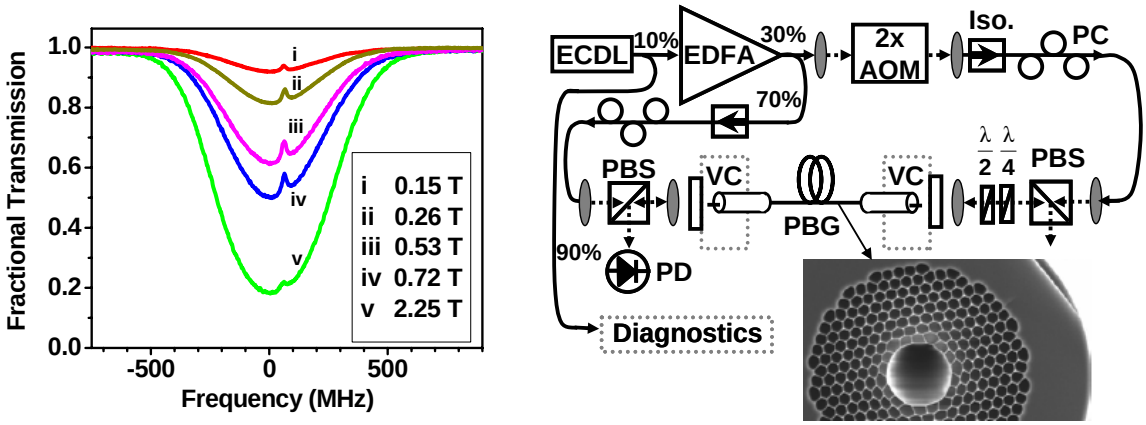

Fig. 1. (left) Fractional transmission versus optical frequency detuning at different gas pressures, for the $^{12}C_2H_2$ P (11) transition with a pump power of 29 mW incident on the fiber. The narrow saturated absorption feature is offset from zero frequency because there is a frequency different between the pump and probe beams, imposed by an acousto-optic modulator (AOM). (right) Schematic of the experimental setup.

The experimental set-up used to realize the saturated absorption spectra is shown in Fig. 1. An extended cavity diode laser (ECDL) emitts ~5 mW, 10% of which is amplified by an IPG Photonics® Erbium-doped fiber amplifier (EDFA) to up to 500 mW. Also shown are an isolator (Iso.), a polarization controller (PC), a polarizing beam splitter (PBS), the vacuum chambers (VC), and a photodetector (PD). The frequency diagnostics include a glass cell filled with $^{12}C_2H_2$ at 50 Torr, in order to locate the relevant transitions, and a Michelson interferometer, used to monitor the laser frequency as it is swept across the transition under study. The polarization is corrected using a half-wave and a quarter-wave retarder before the pump beam is separated from the probe with a PBS.

The theory of saturated absorption spectroscopy is well-known in vapor cells [8]. Beer's law describes the transmission of light through a medium as $I = I_0\, e^{-\alpha s(\nu) l}$, where I_0 is the incident intensity, I is the transmitted intensity, and l is the length of the medium. From the transmitted intensity, we calculate $l\,\alpha_s(\nu)$, as shown in Fig. 2. then $l\,\alpha_s(\nu)$ is fit to an appropriate function, taking into account the Gaussian nature of the Doppler broadened signal and the Lorentzian saturation dip. Figure 3 shows the dependence of the Lorentzian full-width-half-maximum on optical power. Figure 3 also shows the frequency discrimination of the saturated absorption feature, which is the signal height in fractional absorption divided by the signal width in MHz. Larger values indicate increased suitability for an optical frequency reference.

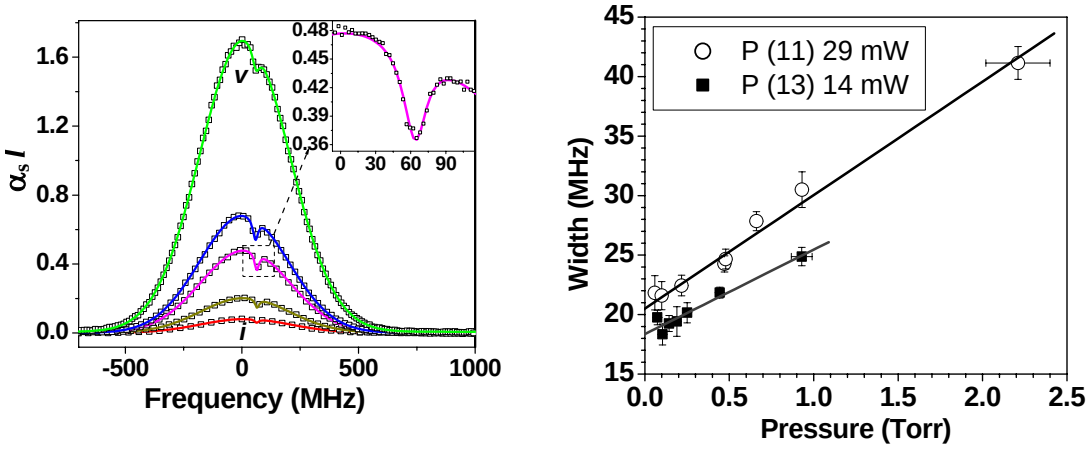

Fig. 2. (left) $\alpha_s l$ calculated with pressure varying from v to i according to the legend of Fig. 1. Solid lines represent fits to the above equation, using the function described above. (right) Width vs. pressure resulting from fits at left.

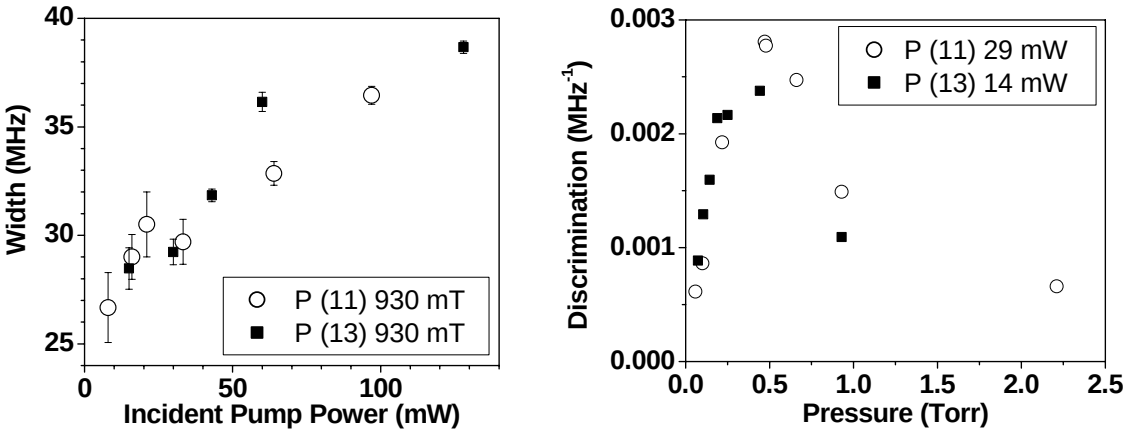

Fig. 3. (left) Width as a function of pump power for both P (11) and P (13) at 0.93 T pressure. (right) Frequency discrimination of the saturation dip, indicating the suitability of the standard for a frequency reference.

We gratefully acknowledge funding from NSF and AFOSR.

References

[1] W. C. Swann and S. L. Gilbert, "Pressure-induced shift and broadening of 1510 - 1540-nm acetylene wavelength calibration lines," J. Opt. Soc. Am. B **17**, 1263 - 1270 (2000).

[2] F. L. Hong, A. Onae, J. Jiang, R. X. Guo, H. Inaba, K. Minoshima, T. R. Schibli, and H. Matsumoto, "Absolute frequency measurement of an acetylene-stabilized laser at 1542 nm," Optics Letters **28**, 2324-2326 (2003), <Go to ISI>://000186734900014.

[3] A. Czajkowski, J. E. Bernard, A. A. Madej, and R. S. Windeler, "Absolute frequency measurement of acetylene transitions in the region of 1540 nm," Applied Physics B-Lasers and Optics **79**, 45-50 (2004), <Go to ISI>://000221675500008.

[4] C. S. Edwards, H. S. Margolis, G. P. Barwood, S. N. Lea, P. Gill, and W. R. C. Rowley, "High-accuracy frequency atlas of $^{13}C_2H_2$ in the 1.5 μm region," Applied Physics B-Lasers And Optics **80**, 977-983 (2005), <Go to ISI>://000230074500007.

[5] F. Benabid, F. Couny, J. C. Knight, T. A. Birks, and P. S. J. Russell, "Compact, stable and efficient all-fibre gas cells using hollow-core photonic crystal fibres," Nature **434**, 488-491 (2005).

[6] S. Ghosh, J. E. Sharping, D. G. Ouzounov, and A. L. Gaeta, "Resonant Optical Interactions with Molecules Confined in Photonic Band-Gap Fibers," Phys. Rev. Lett. **94**, 093902 (2005).

[7] M. Faheem, R. Thapa, and K. L. Corwin, ""Spectral Hole Burning of Acetylene Gas inside a Photonic Bandgap Optical Fiber"," in *Proceedings of Conference on Lasers and Electro-optics*, (Optical Society of America, 2005)

[8] W. Demtröder, *Laser Spectroscopy*: Springer, 1996.

Splicing hollow-core photonic bandgap fibers to step-index fibers using an arc fusion splicer

R. Thapa, K. L. Corwin, B. R. Washburn
Kansas State University, Dept. of Physics, 116 Cardwell Hall, Manhattan, KS 66506
email washburn@phys.ksu.edu, phone: 785-532-2263, fax: 785-532-6606

Abstract: A method for splicing hollow-core photonic bandgap fibers to step-index fiber using a commercial arc fusion splicer has been developed. These splices compare favorably with commercially available splices for nonlinear optical interactions with gases.

OCIS codes: (060.4510) Optical communications; (120.3930) Metrological Instrumentation; (300.1030) Absorption; (230.3990) Microstructure devices;

1. Introduction

The advent of photonic bandgap fiber (PBG) has spurred many studies of nonlinear interactions between light and molecular gases. Raman scattering by hydrogen gas in these fibers allows highly efficient wavelength conversion [1]. Electromagnetically-induced transparency has been observed in acetylene-filled fibers, toward all-optical fiber communications [2]. Saturation spectroscopy, toward higher-accuracy portable optical frequency references, has also been demonstrated [3]. Even linear interactions are significantly enhanced, resulting in the development of gas sensors [4] and Doppler- and pressure-broadened frequency references [1].

Practical devices based on gas-filled PBG fiber require both ends hollow fiber to be sealed. Typically this is accomplished by fusion-splicing to solid-core single mode fiber (SMF), which is challenging due to the fragile PBG fiber. PBG fibers have been sealed after being filled by acetylene gas [1], but this technique relies on the use of an expensive, filament-based fusion splicer, and commercially-available spliced fibers are manufactured with the same technology [5]. Solid-core microstructured fibers have been spliced with arc-splicers [6], and the collapse of air holes in PBG fiber for selective injection has been systematically investigated [7]. However, a simple recipe for splicing PBG fiber to SMF using a conventional arc fusion splicer has until now been lacking. Here we demonstrate a repeatable, robust, low loss (<1.5 dB) splice between a hollow-core PBG fibers and SMF. The performance of this fiber compares favorably with a commercially made spliced fiber in saturation spectroscopy.

2. Fusion splicing hollow-core PBG fiber to SMF

The reason filament splicers are generally preferred for PBG fiber fusion splicing is that they heat more slowly and uniformly. Thus we wish to mimic the filament fusion splicer using an Ericsson 995 electric arc fusion splicer. A multi-step splice procedure was used that involved 1) a short, high current arc and 2) a long, low current arc. Figure 1(a) shows the splicing setup and (b) shows the resulting PBG-SMF splice between a hollow-core PBG of core size 10 μm and Coring SMF-28e®.

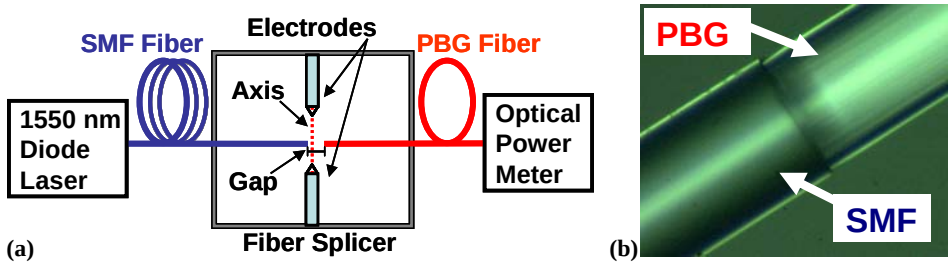

Fig. 1. (a) Experimental set-up for the measurement of splice losses. A tunable diode laser at 1550 nm is used with an optical power meter to measure the coupling during the splice procedure using a commercial arc splicer. (b) A micrograph showing the splice between the SMF and PBG fiber. Picture courtesy of the GaN Group at KSU Physics.

The loss with respect to the butt-coupled throughput was measured during the splicing procedure (Fig. 2). During the splice program the two fibers were briefly butt-coupled (touch point) and then a gap of +10 μm was made. The center position was set to 260, thus the offset of the gap center from the electrodes axis was roughly 5 μm. This offset ensured that less heat was applied to the PBG fiber and prevented a collapse of the air holes. The first fusion current of 10 mA was used for 0.2 s, and then a lower 7 mA current was used for 12 s. During the second current the fibers were overlapped with a gap width (overlap) of -15 μm. (Negative gaps indicate that the fibers are pushed further together than they were when butt-coupled.) Afterwards an independent measurement

determined a total loss of 1.5 dB. The splice was mechanically strong and could be bent in a ~1.5 cm circular radius before breaking.

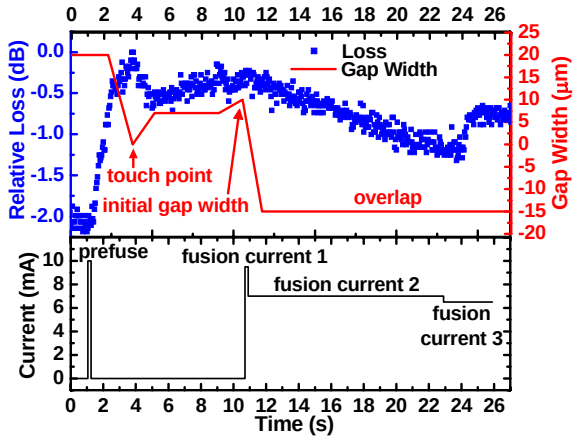

Splice Parameters:	
Initial Gap Width	10 μm
Overlap	-15 μm
Fusion time 1	0.2 s
Fusion current 1	10 mA
Fusion time 2	12 s
Fusion current 2	7 mA
Fusion time 3	3 s
Fusion Current	6.5 mA
Center position	260
(gap center was offset from the electrodes axis by ~5 μm)	

Fig. 2. The measured loss with respect to the butt-couple throughput between the SMF and PBG fiber during the fusion procedure. The gap width was estimated during the time from 10.5 to 11.7 s.

3. Hollow-core PBG fiber to SMF splice for a gas-filled optical frequency reference

To demonstrate the utility of the splice, a 0.78 m length of PBG fiber spliced to SMF (Fiber 1) was evacuated by pumping with a mechanical rough pump on the PBG fiber's open end in a vacuum chamber (Fig. 1(a)). While the pump was on the fiber was able to hold a 15 mT pressure for 12 hours. Then the PBG fiber was filled with acetylene gas in the same vacuum chamber to a pressure of 863 mT. Absorption spectroscopy was performed on the gas in the PBG fiber and a strong absorption feature was observed. The spectra were compared to the same measurement performed with a PBG fiber that had a splice made using a filament fusion splicer (called Fiber 2, purchased from Crystal Fibre). The 2 m length of PBG fiber in Fiber 2 was at 320 mT. Both gas-filled fibers exhibited similar absorption (Fig. 3(b)). Unfortunately, interference with light reflected from the splice limited the visibility of the saturated absorption feature. The exact pathways interfering are not known, but the Fabry-Perot-like fringes had a contrast ratio of ~6% (Fiber 1) and ~7% (Fiber 2), indicating the similarity between the two splices.

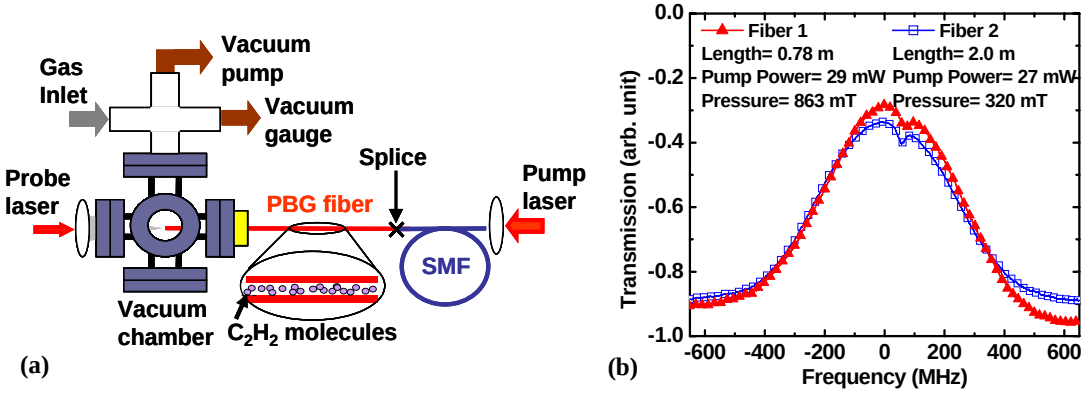

Fig. 3. Chamber used to evacuate and fill the PBG fiber with acetylene gas for the saturated absorption spectroscopy. (b) Saturated absorption spectra of acetylene filled PBG fibers. The fiber with the arc fusion splice (Fiber 1) exhibits a similar absorption profile as the fiber with the filament fusion splice (Fiber 2).

4. References

[1] F. Benabid, F. Couny, J. C. Knight, T. A. Birks, and P. S. J. Russel, "Compact, stable and efficient all-fibre gas cells using hollow-core photonic crystal fibres," Nature, **434**, 488-491 (2005).

[2] S. Ghosh, J. E. Sharping, D. G. Ouzounov, and A. L. Gaeta, "Resonant optical interactions with molecules confined in photonic band-gap fibers," Phys. Rev. Lett., **94**, 093902-1, (2005).

[3] M. Faheem, R. Thapa, and K. L. Corwin, "Spectral hole burning of acetylene gas inside a photonic bandgap optical fiber," presented at Conference on Lasers and Electro-optics, Baltimore, MD (2005).

[4] T. Ritari, J. Tuominen, H. Ludvigsen, J. C. Petersen, T. Sørensen, T. P. Hansen, and J. C. Simonsen, "Gas sensing using air-guiding photonic bandgap fibers," Opt. Express, **12**, 4081 (2004).

[5] Crystal Fibre A/S, http://www.crystal-fibre.com/support/faq.shtm.

[6] B. Bourliaguet, C. Paré, F. Émond, A. Croteau, A. Prouix, and R. Vallée, "Microstructured fiber splicing," Opt. Express, **11**, 3412-17 (2003).

[7] L. Xiao, W. Jin, M. S. Demokan, H. L. Ho, Y. L. Hoo, and C. Zhao, "Fabrication of selective injection microstructured optical fibers with a conventional fusion splicer," Opt. Express, **13**, 9014-9022 (2005).

Spectral Hole Burning of Acetylene Gas inside a Photonic Bandgap Optical Fiber

Mohammed Faheem, Rajesh Thapa, and Kristan L. Corwin
Kansas State University, 116 Cardwell Hall, Manhattan, KS 66506-2601
Phone 785-532-1663, fax785-532- 6806, *corwin@phys.ksu.edu*

Abstract: We have observed saturated-absorption spectra of acetylene gas inside a photonic bandgap fiber. Significant signal sizes observed at low pump powers (< 20 mW) indicate the utility of this technology for portable optical frequency references.

OCIS Codes: 060.2310 (Fiber Optics) ; 300.6460 (Saturation Spectroscopy) ;

Acetylene has been extensively investigated as an optical frequency reference in the near-infrared region of the spectrum. It offers many well-separated transitions, and lacks a permanent dipole moment, which makes it relatively immune to external fields and shifts. Furthermore, the overtone transition corresponding to a symmetric C-H stretch (ν_1) and an antisymmetric C-H stretch (ν_3) gives rise to about 60 lines from 1512 nm – 1544 nm in $^{12}C_2H_2$ and another 60 from 1522 nm -1552 nm in $^{13}C_2H_2$ [1]. Precise realizations of these lines have so far relied on sub-Doppler saturated absorption spectroscopy [2] performed within a power build-up cavity. In 2001, based on measurements by Nakagawa *et al.*[3], the International Committee for Weights and Measures (CIPM) established 53 of these features as optical frequency references with an uncertainty of 200 kHz, and one of them, P(16), with a provisional uncertainty of 100 kHz [4]. Since then, three groups have reduced the uncertainty in the measurement of the P(16) line, as realized in a cavity, by up to 2 orders of magnitude by comparing a laser stabilized to the acetylene transition with a stabilized, Ti:sapphire-based optical frequency comb [5-7].

One of the primary applications of these improved standards is to support the optical telecommunications industry and especially dense wavelength division multiplexing (DWDM). Indeed, many commercially available wavelength measurement devices, such as optical spectrum analyzers, contain acetylene-filled vapor cells certified by the National Institute of Standards and Technology (NIST) to have absorption lines known to 130 MHz, or is some cases 13 MHz [1, 8]. Some applications of DWDM call for increased accuracy in portable frequency references, and some proposed applications will require increasingly accurate references. The vapor cells provided by NIST are limited by Doppler and pressure broadening to their existing levels of accuracy, and cavity-based references are not readily portable. Therefore, new technology is needed to combine the portability of the vapor cells with accuracies approaching that of the gas-filled build-up cavity.

Photonic bandgap fiber [9] offers an excellent medium in which to perform spectroscopy on weak molecular transitions. Due to its low losses (as compared with capillary tubing), light can propagate through a molecular vapor at high intensity over long distances. These features are already being exploited in applications such as gas sensing [10], high-energy soliton propagation [11], and wavelength conversion via rotational Raman scattering [12]. Considerations for signal strength and linewidth are similar in photonic bandgap fiber and in power build-up cavities. Shifts in the cavity-based standards have been observed to contribute on the kHz level to uncertainties [13], and sub-MHz transitions have readily been observed. The two most significant differences between a fiber-based standard as compared to a build-up cavity are the proximity of the fiber surface to the molecules being probed, and the small beam size (~11 μm in the fiber vs. ~500 μm in the cavities). The former is not expected to be observable under the conditions described here. The small beam size results in short interaction times between the molecules and the laser field, giving rise to a transit-time broadening [2] at room temperature in a 10 μm core fiber, of ~50 MHz. Further reduction of the line width in acetylene will require a reduction in this transit time, either by increasing the fiber core size or by preserving coherence between the molecules and the laser field as the molecules bounce off the walls, for example with a wall coating.

We report the observation of sub-Doppler absorption features in molecular gases contained in photonic bandgap fiber. The experimental set-up is shown in Fig. 1. A 56 cm length of commercially-available photonic bandgap fiber (Blaze Photonics HC-1550-02) is attached on each end via a Torr Seal to a metal tube, which is in turn sealed to two separated vacuum chambers by a compression fitting. It is evacuated to ~1 mTorr using a roughing pump, and can then be filled to arbitrary pressures with $^{12}C_2H_2$, as measured with a thermocouple gauge. Light is coupled into and out of each fiber through an AR-coated, wedged window on each chamber using mirrors and a lens mounted to a translation stage. The counter-propagating beams required for saturation spectroscopy are created from a tunable diode laser (~4 mW) at ~1531 nm that is split into two beams. One passes through an acousto-optic

modulator and is used as the probe, while the second is amplified by an erbium-doped fiber amplifier (EDFA) to up to 500 mW. The probe and pump are separated by polarizing beamsplitters, and the probe beam is detected on a photodiode and read out on an oscilloscope. The resulting signals are shown in Fig. 2.

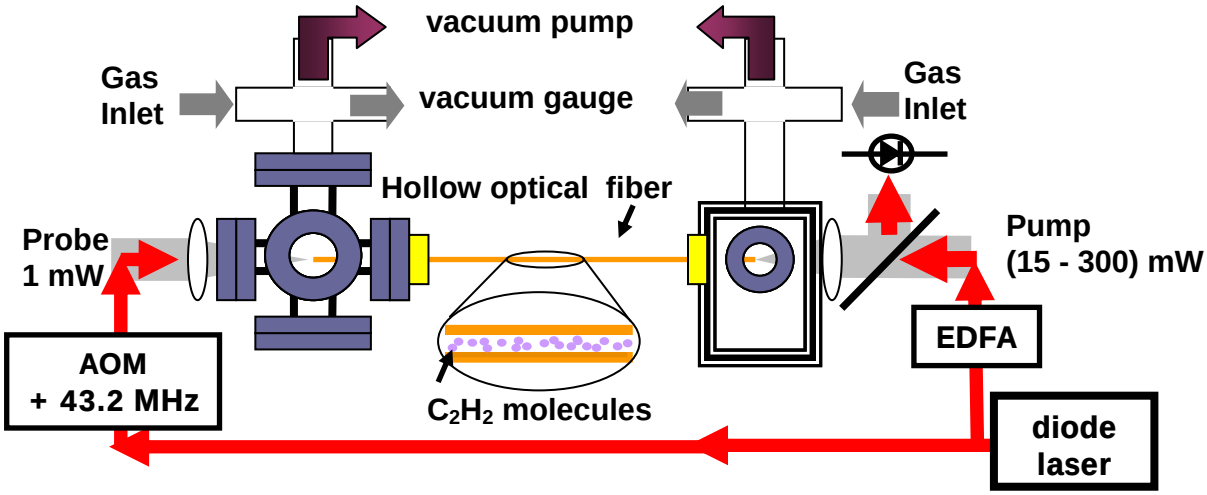

Fig. 1: Schematic drawing of vacuum system and optical beam path for the observation of saturated absorption features in acetylene or other reference gases. The presence of the acousto-optic modulator (AOM) minimizes interference between the probe light and pump light that reflects off the end of the fiber and then strikes the photodetector. The erbium-doped fiber amplifier (EDFA) amplifies the diode laser powers as high as 500 mW, and typically 40% coupling efficiency is achieved into the photonic bandgap fiber.

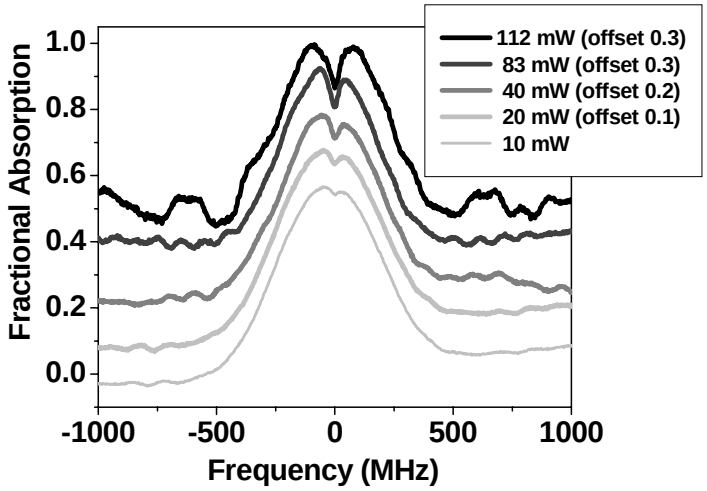

Fig. 2: Saturated absorption spectra of the P(11) feature as a function of pump power. Each signal represents an average of 16 sweeps of ~1s duration across the transition. At higher pump powers, the curves are offset from zero for clarity by the amount indicated in the key. The frequency axis is calibrated using the theoretical Doppler width at room temperature, and the resulting offset of the saturation feature is precisely consistent with half of the AOM frequency, as expected. The increase in noise with pump power is attributed to a residual interference effect between the probe beam and stray pump light. The widths of the features are ~40 MHz, consistent with the expected transit-time broadening.

Saturated absorption spectra over a range of pump powers are shown in Fig. 2, at pressures of ~1.6 Torr. The features have a width of about 40 MHz, consistent with the expected transit-time broadening. The signal size clearly depends on the pump power, consistent with the expected saturation power for this fiber and this transition of ~ 300 mW. Notably, a significant signal is observed at pump powers as low as 10-20 mW. Thus these signals will be observable with off-the-shelf diode lasers, without an EDFA.

Recently, the signal-to-noise ratio on these transitions was significantly improved by increasing the probe power, which diminished the interference effects between the reflected pump power and the probe beam (these effects are seen in Fig. 2 off-resonance as large ripples in the fractional absorption at high pump power). Efforts are ongoing to further narrow the transition by using larger-core fibers, and to investigate the dependence of signal quality on vapor pressure. We intend to seal the fibers on both ends, eliminating the need for the vacuum system. Finally, we plan to measure the optical frequency of these transitions using a frequency comb, looking for possible shifts in optical frequency due to surface interactions or other systematic effects.

We thank Greg Johnson, Mikes Wells and the JRM staff for technical support, and Sarah Gilbert, Dirk Müller, Bill Swann, Kurt Vogel, and Brian Washburn for helpful discussions. This work is funded in part by the National Science Foundation under grant number NSF EPS-0236913 and the State of Kansas through Kansas Enterprise Corporation, as well as Kansas State University.

[1] W. C. Swann and S. L. Gilbert, "Pressure-induced shift and broadening of 1510 - 1540-nm acetylene wavelength calibration lines," J. Opt. Soc. Am. B, **17**, 1263 - 1270 (2000).

[2] W. Demtröder, *Laser Spectroscopy*. (Springer, 1996).

[3] K. Nakagawa, M. d. Labachelerie, Y. Awaji, and M. Kourogi, "Accurate optical frequency atlas of the 1.5-μm bands of acetylene," J. Opt. Soc. Am. B, **13**, 2718 - 2714 (1996).

[4] T. J. Quinn, "Practical realization of the definition of the metre, including recommended radiations of other optical frequency standards (2001)," Metrologia, **40**, 103 (2003).

[5] F.-L. Hong, A. Onae, J. Jiang, R. Guo, H. Inaba, K. Minoshima, T. R. Schibli, H. Matsumoto, and K. Nakagawa, "Absolute frequency measurement of an acetylene-stabilized laser at 1542 nm," Opt. Lett., **28**, 2324-2326 (2003).

[6] C. S. Edwards, H. S. Margolis, G. P. Barwood, S. N. Lea, P. Gill, G. Huang, and W. R. C. Rowley, "Absolute frequency measurement of a 1.5-μm acetylene standard by use of a combined frequency chain and femtosecond comb," Opt. Lett., **29**, 566-568 (2004).

[7] A. Czajkowski, J. E. Bernard, A. A. Madej, and R. S. Windeler, "Absolute frequency measurement of acetylene transitions in the region of 1540 nm," Applied Physics B-Lasers and Optics, **79**, 45-50 (2004).

[8] S. L. Gilbert and W. C. Swann, "Acetylene $^{12}C_2H_2$ absorption reference for 1510 nm to 1540 nm Wavelength Calibration -- SRM 2517a,"Nat. Inst. Stand.Technol. Spec. Publ. 260-133 (2001).http://www.boulder.nist.gov/div815/81503_pubs/WSDocs/SP260-133-01ed.PDF

[9] J. C. Knight, J. Broeng, T. A. Birks, and P. S. J. Russell, "Photonic Band Gap Guidance in Optical Fibers," Science, **282**, 1476-1478 (1998).

[10] T. Ritari, J. Tuominen, H. Ludvigsen, J. C. Petersen, T. Sørensen, T. P. Hansen, and H. R. Simonsen, "Gas sensing using air-guiding photonic bandgap fibers," Optics Express, **12**, 4081 (2004).

[11] D. G. Ouzounov, F. R. Ahmad, D. Müller, N. Venkataraman, M. T. Gallagher, M. G. Thomas, J. Silcox, K. W. Koch, and A. L. Gaeta, "Generation of Megawatt Optical Solitons in Hollow-Core Photonic Band-Gap Fibers," Science, **301**, 1702-1704 (2003).

[12] F. Benabid, G. Bouwmans, J. C. Knight, P. S. J. Russell, and F. Couny, "Ultrahigh Efficiency Laser Wavelength Conversion in a Gas-Filled Hollow Core Photonic Crystal Fiber by Pure Stimulated Rotational Raman Scattering in Molecular Hydrogen," Phys. Rev. Lett., **93**, 123903-1 (2004).

[13] A. Czajkowski, A. A. Madej, and P. Dube, "Development and study of a 1.5 μm optical frequency standard referenced to the P(16) saturated absorption line in the (v(1)+v(3)) overtone band of $^{13}C_2H_2$," Optics Communications, **234**, 259-268 (2004).

Reflected Pump Technique for Saturated Absorption Spectroscopy inside Hollow Photonic Bandgap Fibers

Kevin Knabe,[1] Rajesh Thapa,[1] Brian R. Washburn,[1] and Kristan L. Corwin[1,*]

[1]*Kansas State University, Dept. of Physics, 116 Cardwell Hall, Manhattan, KS 66506*

[*]*Corresponding author: corwin@phys.ksu.edu*

A simplified setup has been implemented for saturated absorption spectroscopy of acetylene-filled photonic bandgap fibers (PBGF) using reflections from a splice interface between PBGF and single mode fiber (SMF). We compare the sub-Doppler feature's dependence on pressure and power with a method where the pump and probe beam enter the fiber at opposing ends. Additionally, a frequency modulation technique is used to lock a diode laser to a transition in the P-branch of the $\nu_1 + \nu_3$ overtone. This is an important step toward realizing an all-fiber frequency reference in the near-IR.

OCIS codes: (300.6460) Spectroscopy, saturation; (060.2310) Fiber optics; (060.4510) Optical communications; (120.3930) Metrological Instrumentation; (300.1030) Absorption; (230.3990) Microstructure devices.

1. Introduction

Hollow-core photonic bandgap fibers (PBGF) exhibit low loss, and can be filled with liquids or gases, facilitating nonlinear interactions between light and a gas or liquid of interest. Several types of sub-Doppler resonant interactions with molecular gases have been observed in these fibers [1], including electromagnetically induced transparency (EIT) [2] and saturated absorption spectroscopy [3-5]. Sealed, gas-filled PBGF cells have formed the basis for all-fiber saturated

absorption spectroscopy [6, 7] and are suitable for portable molecular optical frequency references. EIT and saturated absorption spectroscopy have also been observed in Rb vapors confined inside PBG fibers [1, 2] and antiresonant reflecting optical waveguides (ARROWs) [8].

Saturated absorption spectroscopy can be used in a configuration where the probe beam is created by retro-reflecting the pump beam back through the cavity using a mirror external to the cavity [4, 9]. It was found that by splicing PBGF to single mode fiber (SMF) [10] (in a step towards making a sealed, gas-filled fiber cell), a Fresnell reflection is created from the air-glass fiber interface. Upon investigating the signal quality in this half-cell fiber, we found that this Fresnell reflection is suitable for both saturated absorption spectroscopy and frequency modulation (FM) spectroscopy [11, 12].

2. Reflected Pump Experimental Setup

The differences and similarities between the traditional two-beam technique and the (retro) reflected pump technique are illustrated schematically in Fig. 1. The reflected pump technique requires approximately half of the optical components of the two-beam method [4, 9], as well as fewer polarization optics.

Saturated absorption spectroscopy requires a pump beam and a counter-propagating probe beam in order to see the sub-Doppler absorption feature. The two beam method accomplishes this by splitting a laser source into two separate beams that are coupled into opposite ends of a PBGF [5]. Both beams originate from the output of an erbium doped fiber amplifier (EDFA) whose input is an external cavity diode laser (ECDL) at ~1.53 μm. The output of the EDFA is split to create the pump and probe beams, which are linearly polarized after passing through separate polarizing beam splitters (PBS). Each beam is then coupled through a window (anti-reflection coated on one side) into the PBGF which resides in a vacuum chamber. The fiber used

here is described in Table 1 as fiber F1. The probe beam passes through the fiber from right to left, and because its polarization is made to be orthogonal to the pump, it is redirected by PBS 1 onto the photodetector. The pump similarly passes through the fiber from left to right.

In the two beam technique, spurious reflections can create interference and degrade signal quality. Frequency shifting and careful polarization management are used to minimize the impact of this interference. Specifically, the probe beam is frequency-shifted by 100 MHz in a double-passed acousto-optic modulator (AOM) so that any interference between stray pump light and the probe occurs at high frequencies to which the photodetector does not respond. Furthermore, the fiber acts as a waveplate and adds a variable polarization rotation to beams propagating through the fiber, allowing PBS 1 to direct spurious pump light onto the photodetector. Thus the waveplates are arranged such that the exiting probe beam and any reflected pump light are orthogonally polarized at PBS 1.

In contrast, the reflected pump technique minimizes interference by eliminating one of the input beams. Once the pump beam traversed the PBGF (Fig. 1b), a small portion of the pump beam retro-reflects backwards at the splice interface between the PBGF and SMF. This reflected light becomes the probe beam. A non-polarizing beam splitter is used to obtain this saturated absorption signal once the probe beam exits the fiber.

Surprisingly, some reflections and resulting interference arose when the SMF fiber in Fig. 1b was terminated with an angled connector. These reflections were eliminated by splicing to an isolator or circulator with a return loss of at least 45 dB. The majority of data presented here were taken with an isolator in place. However, the data with fiber F3 were taken without this isolator, and the interference resulting from reflections was averaged out by sweeping the laser frequency while manually perturbing the fiber. Data taken with the isolator yielded widths that

agree with the data taken with the perturbation. Additional off-resonant interference can be attributed to wavelength-dependent coupling between the core and lossy surface modes in the PBGF [4].

3. Reflected Pump Results and Data Analysis

We measured saturated absorption spectra using the reflected pump technique near 1532 nm. For this, the ECDL was swept across the P(11) or P(13) $\nu_1+\nu_3$ overtone transition in acetylene. The resulting fractional transmission was converted into a frequency-dependent Naperian absorbance $\alpha(\nu)\cdot l$ (hereafter known only as absorbance) using Beer's Law: $P(\nu,l) = P_0 \cdot \exp(-\alpha(\nu)\cdot l)$ where P_0 is the incident power, P is the transmitted power, and l is the length of the fiber. Figure 2 shows experimentally measured absorbance as a function of laser frequency for different powers in fiber F2. These data were fit to the following effective absorbance [13]:

$$\alpha_e(\nu)\cdot l = A_g \cdot e^{-2(\frac{\Delta\nu}{\sigma})^2} \cdot [1 - A_l \cdot \frac{(w)^2}{4(\Delta\nu)^2 + (w)^2}] \qquad (1)$$

where A_g is the peak absorbance, $(A_g)(A_l)$ is the height of the sub-Doppler feature, σ is the Doppler width, and w is the sub-Doppler Lorentzian width. Additional sinusoidal and linear terms were added to fit the background of the spectrum.

Equation 1 is the same function used to fit the data resulting from the two-beam technique [5]. We expect A_g to be a factor 2 larger and A_l a factor two smaller in the reflected-pump technique than in the two-beam technique for the same gas pressure and fiber length, in the limit of low pump power. This arises from the creation of the probe beam by the pump beam after it has traversed the length of the PBGF (see Fig. 1b). At low powers, this leads to the probe's

absorbance being approximately twice as large as in the two-beam case because it travels twice the path length (neglecting propagation effects). However, when the pump power approaches the saturation limit, the fractional transmission of the pump beam increases. Mathematically, we approximate the absorbance, neglecting propagation effects, as:

$$A_g = A_{g0}(1 + (1 + P/P_S)^{-1/2}) \tag{2}$$

where A_{g0} is the peak absorbance of the pump beam and P_S is the saturation power [13]. In contrast, $A_g = A_{g0}$ for the two beam probe absorbance. The functional dependence of Eq. (2) is observed in Fig. 2 as a reduction in the maximum value of $\alpha(\nu) \cdot l$ with increasing power, and equivalently in the inset as a decreasing value of A_g with increasing power. The dashed line in Fig. 2 (inset) shows a fit using Eq. (2) with P_S fixed at 23 mW as measured in Ref. [4] in a transit time dominated regime similar to this system.

Figure 3a shows how the FWHM of the sub-Doppler feature changes with transmitted pump power where corrections are made for the directionally dependent splice loss given in Table 1. The open symbols represent data taken in fiber F1 using the two-beam technique, while the closed symbols represent data taken in fiber F3 using the reflected pump technique, where pressures and fiber lengths were chosen to give similar absorbances at low power. Errors bars were calculated by a chi-squared fitting routine, and underestimate the overall uncertainty in the measurement. The difference between the widths of the two beam system and the reflected pump system are due to pressure broadening effects of working at two different pressures.

When comparing these two systems for use as wavelength references, discrimination, D, is a useful figure of merit [5]. It is related to the slope of the absorption signal used to stabilize a laser, where a steeper slope in general provides a better frequency reference. It is defined as $D =$

$C/w = (\exp(A_g(1-A_l)) - \exp(A_g))/w$ where C is similar to the "contrast" $C(p)$ of Ref. [14]. Figure 3b compares D for the two techniques. Even though the widths differ, the reflected pump technique exhibits similar D values.

It is helpful to compare the discrimination achievable using other techniques. Previously in Ref. [4], values of D were given erroneously in $(\text{kHz})^{-1}$ rather than $(\text{GHz})^{-1}$. Therefore we give the comparison again here. Other options for acetylene-based frequency references include a side-lock to Doppler-broadened absorption line or a power build-up cavity [15]. For the Doppler-broadened feature of Ref. [6], $C \sim 0.6$, $w \sim 450$ MHz, and $D \sim 1.3\ (\text{GHz})^{-1}$. For the cavity-based saturated absorption of Ref. [15], $C \sim 0.7$, $w \sim 0.8$ MHz, and $D \sim 88\ (\text{GHz})^{-1}$. Thus either of the two techniques offers a higher D than the Doppler-broadened feature, but are more than an order of magnitude below the cavity-based references.

4. Diode Laser Locking Using FM Spectroscopy

To demonstrate the reflected pump's suitability to interrogate a frequency reference, FM spectroscopy was used to lock a cw laser to the acetylene sub-Doppler feature. This particular method was chosen because of its derivative-like error signal, high bandwidth, and ease of implementation (Fig. 4). A digital synthesizer directly modulates the current in the diode laser at a modulation frequency of f_{mod} = 15 MHz. The modulated output light is then amplified by an EDFA for use in the reflected pump setup. The coupling into the PBGF contained in the vacuum chamber is the only free space alignment in this setup, and can be eliminated by using a gas-filled fiber cell. The probe beam from the reflected pump setup is then directed onto a fast photodetector. Next, a Bias-T is used as a high-pass filter and the resulting signal is mixed with f_{mod} created from a second digital synthesizer, the phase of which can be adjusted directly on the instrument to reveal the absorption or the dispersion of the reflected pump setup. The output

from the mixer is then sent through a low-pass filter whose corner is below f_{mod}. This signal is used as an error signal which is sent through two different loop filters to control the current and the piezo-electric transducer (PZT) in the external cavity of the diode laser.

Figure 4 also shows the typical modulated probe fractional transmission and error signal generated by this setup. The error signal shows a dispersive signal which has a DC offset, most probably due to the uneven background (as seen on either side of the absorption feature). We have locked the laser to ±1 MHz peak-to-peak deviation as measured in-loop, and are limited by technical noise and the slow response of our particular diode laser. To improve the quality of the lock, we plan to replace the diode laser with a narrow-line fiber laser, and use a fiber-based electro-optic modulator for sideband generation instead of modulating the laser current directly.

5. Conclusion

We have demonstrated a simplified reflected-pump method to implement saturated absorption spectroscopy on acetylene inside PBGF. The absorption signal of the reflected pump technique contains power-dependent features that are unique to this method, and in the limit of high power the absorbance becomes that of the two-beam method. The characteristic width and depth of the Lorentzian component of the absorbance are comparable to that of the traditional two-beam technique. Thus, discrimination is preserved while sources of interference are eliminated and the optical implementation is simplified. FM spectroscopy was added to peak-lock a diode laser to the absorption feature, toward the development of portable optical frequency references. Incorporation of a fully-sealed PBGF cell will require careful management of additional reflections. This method should readily be extendable to other gases and to ARROW waveguides [8].

We thank Kurt Vogel at Precision Photonics Corp. for designing the FM locking scheme, the James R. Macdonald Laboratory staff for technical assistance, and Holger Schmidt and Larry Weaver for helpful discussions. This material is based upon work supported by the Air Force Office of Scientific Research under contract No. FA9950-05-1-0304 and the National Science Foundation under Grant No. ECS-0449295.

References and links

1. S. Ghosh, J. E. Sharping, D. G. Ouzounov, and A. L. Gaeta, "Resonant optical interactions with molecules confined in photonic band-gap fibers," Phys. Rev. Lett. **94**, 093902 (2005).
2. F. Benabid, P. S. Light, F. Couny, and P. S. Russell, "Electromagnetically-induced transparency grid in acetylene-filled hollow-core PCF," Opt. Express **13**, 5694-5703 (2005). http://www.opticsexpress.org/abstract.cfm?id=85223.
3. J. Hald, J. C. Petersen, and J. Henningsen, "Saturated Optical Absorption by Slow Molecules in Hollow-Core Photonic Band-Gap Fibers," Phys. Rev. Lett. **98**, 213902 (2007).
4. J. Henningsen, J. Hald, and J. C. Petersen, "Saturated absorption in acetylene and hydrogen cyanide in hollow-core photonic bandgap fibers," Opt. Express **13**, 10475-10482 (2005). http://www.opticsexpress.org/abstract.cfm?id=86652.
5. R. Thapa, K. Knabe, M. Faheem, A. Naweed, O. L. Weaver, and K. L. Corwin, "Saturated absorption spectroscopy of acetylene gas inside large-core photonic bandgap fiber," Opt. Lett. **31**, 2489-2491 (2006).
6. F. Benabid, F. Couny, J. C. Knight, T. A. Birks, and P. S. Russell, "Compact, stable and efficient all-fibre gas cells using hollow-core photonic crystal fibres," Nature **434**, 488-491 (2005).
7. P. S. Light, F. Couny, and F. Benabid, "Low optical insertion-loss and vacuum-pressure all-fiber acetylene cell based on hollow-core photonic crystal fiber," Opt. Lett. **31**, 2538-2540 (2006).
8. W. G. Yang, D. B. Conkey, B. Wu, D. L. Yin, A. R. Hawkins, and H. Schmidt, "Atomic spectroscopy on a chip," Nature Photonics **1**, 331-335 (2007).

9. M. Weel and A. Kumarakrishnan, "Laser-frequency stabilization using a lock-in amplifier," Can. J. Phys. **80**, 1449-1458 (2002).

10. R. Thapa, K. Knabe, K. L. Corwin, and B. R. Washburn, "Arc fusion splicing of hollow-core photonic bandgap fibers for gas-filled fiber cells," Opt. Express **14**, 9576-9583 (2006). http://www.opticsexpress.org/abstract.cfm?id=116356.

11. G. Bjorklund, M. Levenson, W. Lenth, and C. Ortiz, "Frequency Modulation (FM) Spectroscopy," Appl. Phys. B **32**, 145-152 (1983).

12. R. Drever, J. Hall, F. Kowalski, J. Hough, M. Ford, A. Munley, and H. Ward, "Laser Phase and Frequency Stabilization Using an Optical Resonator," Appl. Phys. B **31**, 97-105 (1983).

13. W. Demtröder, *Laser Spectroscopy: Basic Concepts and Instrumentation* (Springer, 1996).

14. M. Delabachelerie, K. Nakagawa, and M. Ohtsu, "Ultranarrow $^{13}C_2H_2$ saturated-absorption lines at 1.5 μm," Opt. Lett. **19**, 840-842 (1994).

15. A. Czajkowski, A. A. Madej, and P. Dube, "Development and study of a 1.5 μm optical frequency standard referenced to the P(16) saturated absorption line in the (ν_1+ ν_3) overtone band of $^{13}C_2H_2$," Opt. Commun. **234**, 259-268 (2004).

Figures

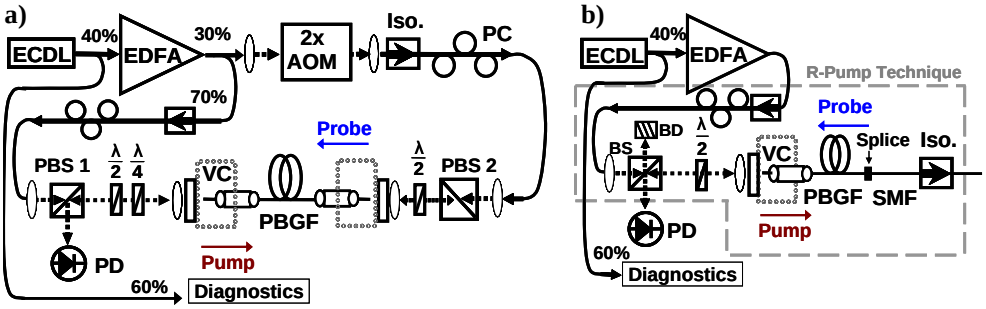

Fig. 1. Schematic of a) the traditional two-beam configuration for saturated absorption spectroscopy and b) the retro-reflected pump technique, where the probe beam is created at the splice interface between the PBGF and SMF. Solid lines indicate laser beams contained within fibers, whereas short dashed lines indicate beams in free-space. Long dashed gray lines indicate the reflected pump technique, which is later referred to in Figure 4. Beam dump (BD), beamsplitter (BS), Isolator (Iso.), Polarization Controller (PC), Photodetector (PD), Vacuum Chamber (VC).

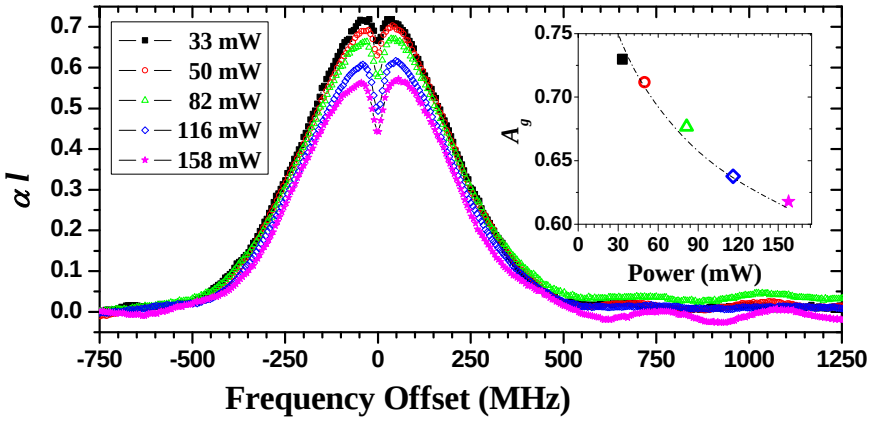

Fig. 2. Absorption spectra of the C_2H_2 $\nu_1+\nu_3$ P(11) vibrational line at an optical wavelength of ~1.53 μm for fiber F2 at a pressure of 0.50 Torr for the listed pump powers. Each trace is an average of 8 scans while sweeping the frequency at ~4 GHz/s. The inset picture is graph of A_g versus power with a fit to Eq.(2) using a saturation power of 23 mW [4].

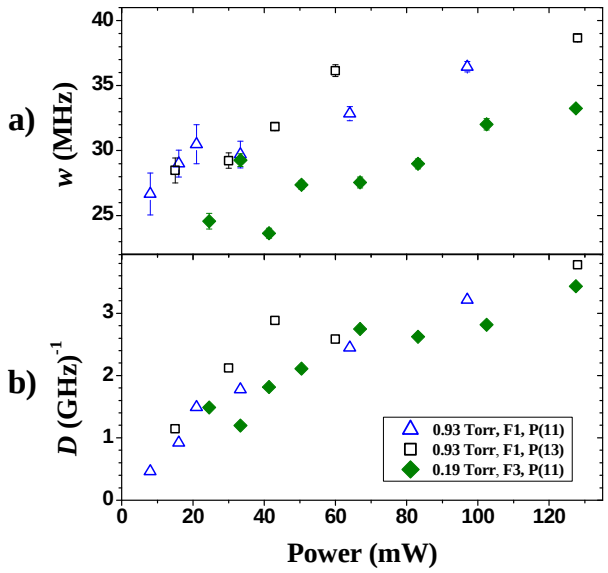

Figure 3. a) Sub-Doppler widths vs. power extracted from fits of Eq. (1) to spectra such as those shown in Fig. 2. The pressure, fiber, and transition used in each measurement are listed in the legend. Open and solid symbols indicate the two-beam and reflected pump setups, respectively. b) The discrimination *D* versus power, for the same measured spectra.

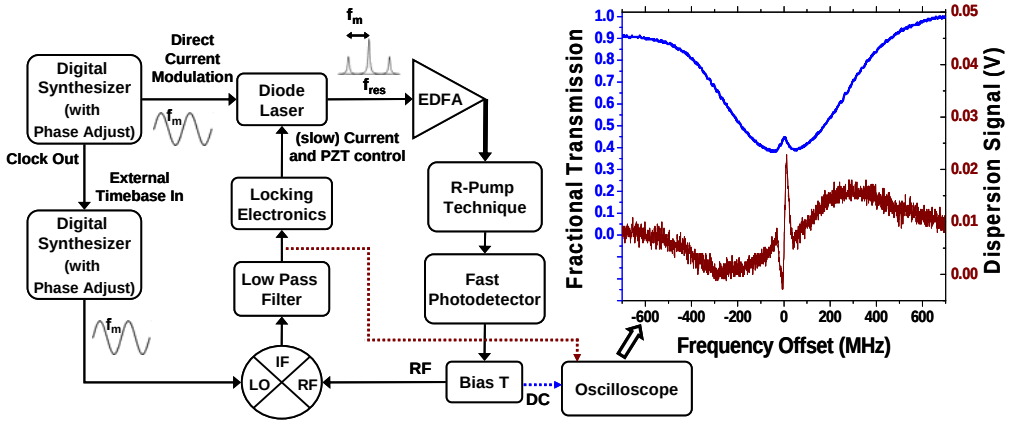

Figure 4. Schematic of diode laser locking using FM spectroscopy with the reflected pump technique. The inset picture to the right is an example of the typical transmission spectrum (blue) and error signal (maroon) generated with this setup.

Tables

Table 1: Fibers used for saturated absorption spectroscopy, spliced using the technique described in Ref. [10].

Fiber	PBGF Length (m)	Technique	Type	Splice Loss (dB) SMF → PBGF	Splice Loss (dB) PBGF → SMF
F1	0.78	Two beam	19-cell PCF*	not applicable	not applicable
F2	0.40	Reflected pump	19-cell PCF*	0.3-0.5	> 2.0
F3	2.60	Reflected pump	19-cell PCF*	0.3-0.5	> 2.0

*19 cell PCF with ~20μm core. Part number HC19-1550-01 from Crystal Fibre A/S.